## General Disclaimer

## One or more of the Following Statements may affect this Document

- This document has been reproduced from the best copy furnished by the organizational source. It is being released in the interest of making available as much information as possible.

- This document may contain data, which exceeds the sheet parameters. It was furnished in this condition by the organizational source and is the best copy available.

- This document may contain tone-on-tone or color graphs, charts and/or pictures, which have been reproduced in black and white.

- This document is paginated as submitted by the original source.

- Portions of this document are not fully legible due to the historical nature of some of the material. However, it is the best reproduction available from the original submission.

# FEASIBILITY STUDY OF A SPACECRAFT MOUNTED METEOROID RADAR SYSTEM

## FINAL TECHNICAL REPORT

## VOLUME II. SYSTEM IMPLEMENTATION

TECHNICAL REPORT NO. U1-943500-1

DECEMBER 1968

PREPARED UNDER CONTRACT NO. NAS 9-7822

by

TEXAS INSTRUMENTS INCORPORATED
EQUIPMENT GROUP
13500 NORTH CENTRAL EXPRESSWAY
DALLAS, TEXAS 75222

for

NATIONAL AERONAUTICS & SPACE ADMINISTRATION
MANNED SPACECRAFT CENTER

NASA CR 92482

# FEASIBILITY STUDY OF A SPACECRAFT MOUNTED METEOROID RADAR SYSTEM

## FINAL TECHNICAL REPORT

## VOLUME II. SYSTEM IMPLEMENTATION

TECHNICAL REPORT NO. U1-943500-1

DECEMBER 1968

PREPARED UNDER CONTRACT NO. NAS 9-7822

by

TEXAS INSTRUMENTS INCORPORATED
EQUIPMENT GROUP
13500 NORTH CENTRAL EXPRESSWAY
DALLAS, TEXAS 75222

for

NATIONAL AERONAUTICS & SPACE ADMINISTRATION
MANNED SPACECRAFT CENTER

# FOREWORD

| | |
|---|---|
| SPONSORING ACTIVITY | National Aeronautics & Space Administration<br>Manned Spacecraft Center<br>Houston, Texas |
| TECHNICAL MONITOR | Mr. Kenneth Baker / TG2<br>Space Sciences Procurement Branch |
| CONTRACT NUMBER | NAS 9-7822 |
| SUBMITTED | December 1968 |

# ACKNOWLEDGEMENT

This study was conducted under the technical direction of Mr. Mark W. Smith who supervised preparation of the final report. Volume II was compiled by Mr. B.D. Turpin. The following individuals contributed significantly to the technical results obtained in this study:

Mr. W.E. Brasher
Dr. R. E. Lawrie
Mr. F.J. Lewis
Mr. M.W. Smith
Mr. B.D. Turpin

Additional contributors were:

Mr. J.R. Brennan
Dr. E.M. Schall
Mr. R.E. Voges

TABLE OF CONTENTS

## LIST OF TABLES

Volume II

# SECTION I

# DESIGN OF THE SELECTED RADAR

## A. INTRODUCTION AND SUMMARY

Volume I of this report discusses the detection and measurement capabilities of several candidate meteoroid radar systems. A particular type of radar was selected for further detailed study and the radar parameters were selected so as to maximize the number of particles detected consistent with physical limitations imposed by the space environment. The optimum design was then modified to provide velocity and radar cross section measurement capabilities.

This volume is an addendum to the analytical analysis performed in Volume I. Presented is a sample and suggested radar system design based upon the optimum system as determined by the results reported in Volume I. Attention has been focused on Mission 2, the asteroid belt fly-through mission, because of the large detection advantage resulting from this choice.

The radar discussed is a noncoherent pulsed radar employing a pair of nontracking, frequency-scanned pencil beams for making velocity measurements. The nominal design parameters of the radar system selected for detailed design are listed below.

### 1. Antenna

The system will employ a pair of symmetrical pencil beam antennas having nominal beamwidths of 0.5 degree. The two beams will be scanned in parallel planes separated by a 10-degree interior angle as is shown in Figure I-1. Each beam will be capable of sequentially observing 50 contiguous scan positions. The dwell time at each location will correspond to the inverse of the pulse repetition frequency. Electronic scanning will be employed. Frequency scanning has been selected to minimize beam steering complexity. The scan pattern is a simple raster scan with adjacent beam positions overlapping at the 3-dB antenna gain points. Both beams move together and in parallel.

The aperture required to achieve the 0.5 by 0.5-degree beam is substantial (6 feet by 7 feet) and requires an erectable antenna for a Mariner '69 sized spacecraft. The antenna is fixed to the spacecraft, and thus is near optimum only for Mission 2 where no mechanical scanning is required to achieve the desired normal aspect between antenna and the nominal particle directions throughout the one-year period.

No intrabeam angle measurements are made. Adding angle measuring techniques such as amplitude or phase monopulse would significantly complicate antenna design. It is doubtful that the selected antenna

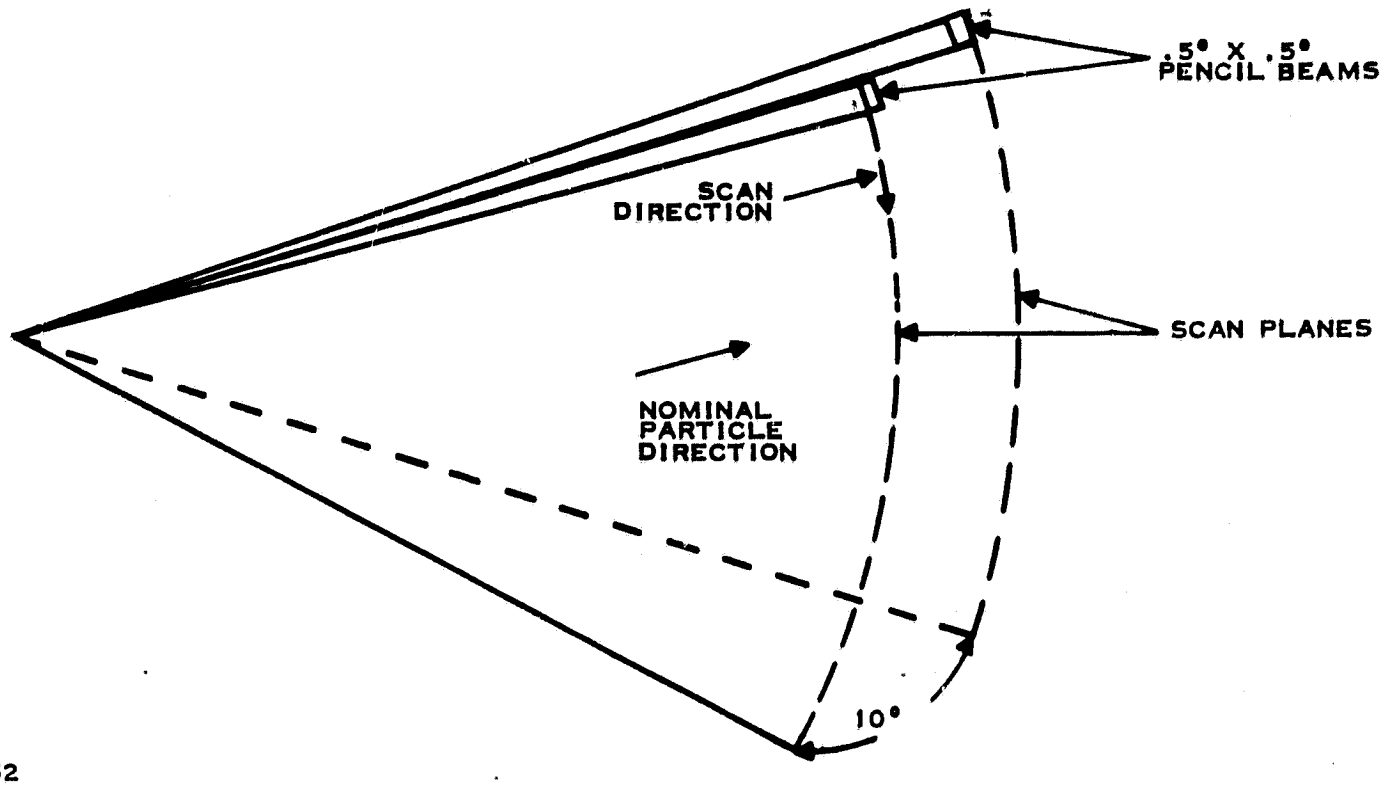


Figure I-1. Antenna Scan Geometry

technique could be used; a different antenna technique would be required. A space-fed planar array employing phase shift electronic scanning appears theoretically most attractive. However, obtaining the desired 0.5 by 0.5-degree beamwidth with a space-fed array could easily double the system weight and volume. If the radar cross section accuracy resulting from the selected radar system is not satisfactory, such an alternative would have to be considered. The selected radar design does not include a provision for obtaining intrabeam angle measurements because the resulting radar design would be of questionable real value.

2. Transmitter

The transmitter is a standard pulsed radar design employing a TWT as the final power amplifier. An average radiated power of 50 watts is assumed. A 0.5-μsec pulse having 5-kilowatt peak power and a pulse repetition frequency of 20,000 pps is used. The pulse is split into two equal pulses and radiated simultaneously by the two antennas. The nominal 15-GHz carrier frequency is varied in 10-MHz steps between pulses to achieve the desired beam scanning. The chosen 50-watt average power system requires a prime power of 320 watts (total).

3. Receiver

The receiver is more complicated than the usual radar receiver because of the linearity required to measure particle radar cross section over a 50-dB dynamic range. Because of the linearity requirements, the desired receiver signal gain and frequency selectivity is accomplished in seven stages of serial amplification with appropriate circuit monitoring to sense any circuit saturation which may occur. Two identical receiver IF filters are used. The IF bandwidth has been selected to be 2.2 MHz, slightly larger than that required by the transmitted pulse to account for the doppler frequency shifts encountered.

The suggested radar design, which corresponds closely to the optimum system discussed in Volume I, is fully described in the body of this report. It is shown that there is not sufficient prime power available from the solar cell panels of the Mariner '69 to supply a radar capable of detecting a modest number of meteoroids plus supply the other necessary power needs. This is in part due to the large sun-spacecraft distances encountered in regions of high meteoroid density and the reciprocal relationship between this distance squared and solar cell power output. There also seems little possibility of obtaining the required power from the Mariner '69 spacecraft by increasing the solar cell panel area.

It is also shown that the solar cell panel area of a Voyager-type spacecraft must be increased three-fold to supply the required power. However, this appears to be feasible.

The telemetry requirements are at a minimum with the present design, even though no measurement computations are performed on the spacecraft. There will be approximately 12,000 bits of information per year for both particle characterization and housekeeping, and thus would require no special data handling technique not already available on a Mariner '69 type spacecraft.

The basic system reliability analysis indicated an estimated system reliability of 8 percent for one year operation. This is a good reliability figure for maintenance-free, one-year radar operation. However, with selected redundancy this reliability could be increased to 38 percent. This selected redundancy would increase both the system volume and weight by approximately 35 percent.

The basic volume and weight requirements of the electronics system, excluding the antenna, are a packaged volume of 1 cubic foot, a weight of 64 pounds, and a prime power requirement of 320 watts. The antenna has a launch volume of 81 cubic feet and a total weight of 71 pounds. These values do not include this selected redundancy for reliability improvement.

4. Required Development Efforts

The radar system implementation described in Volume II was selected specifically to be capable of implementation with state-of-the-art components. No special development efforts are required for most of the radar system.

Two areas where development efforts will be required are the antenna and the TWT final power stage and associated power supplies. It is estimated that a minimum one-year development and reliability testing program would be required to design, fabricate, and test the type of TWT subsystem specified. If extensive reliability testing was conducted, the time could easily grow to one and one-half years.

The antenna design would also require a development program due to the unusual frequency scanning and deployment requirements. The estimated design, fabrication, and preliminary testing would require 9 to 12 months. Environmental tests of deployment, etc., would add an additional six months for a total of about one and one-half years.

The remaining electronics subsystems are all fabricated using standard techniques which are readily available.

The estimated system reliability, while very good for complex radar systems of the type described, could certainly be improved by a careful reliability analysis and testing program with suggested changes and remedial action if necessary. Such a study could be conducted in parallel with detailed system design.

A non-radar area where developmental effort would be required is that of spacecraft power supply subsystems. Several developments of this type are now under preliminary consideration in the industry. It should be recognized that a meaningful meteoroid radar cannot be fabricated as an add-on experiment for any existing spacecraft because of the significant prime power levels required and the increased sun-spacecraft distances favorable for detecting a moderate number of particles.

## B. RADAR SYSTEM DESCRIPTION

This section acquaints the reader with the overall system in preparation for the detailed discussion of the separate subsystems which will be undertaken in the following section.

Concomitant with satisfying the requirements indicated by the particle detection analysis was an attempt to minimize the demands of the radar system upon the spacecraft prime systems by a prudent choice of fabrication techniques. The radar system chosen for the fabrication study was the shortpulse system employing a pair of frequency-scanned beams. The greater the separation between the two beams, the more accurate can the particle

trajectory be measured. Also, maximum effort was put forth to obtain the maximum accuracy in measuring the strength of the return signal level, thus assuring that a detected particle would be characterized as accurately as possible.

The functional block diagram of such a system is illustrated by Figure I-2. Discussion of the system operation begins with the frequency synthesizer. Due to the rapidity with which the antenna beam must be scanned, mechanical scanning or electrical phase shift scanning cannot conveniently be used. Mechanical scanning of the antenna cannot be used because of the high scan rates required. Electrical phase shift scanning is also on the border line between being feasible and unfeasible because of the large computational rates required to generate and distribute the phase shift commands. Current state-of-the-art phase shifters would also add considerable weight, complexity, and power dissipation to the system.

The alternative was to employ frequency scanning. With frequency scanning the frequency of the signal source is varied to achieve the desired beam position. Scanning difficulties have thus been transferred to the initial antenna design and fabrication and to development of a frequency synthesizer. Neither problem is insurmountable although the antenna design would require a developmental effort.

Several problems typical of frequency-scanned arrays such as limited antenna signal bandwidth and involuntary array scanning due to received signal doppler shifts have been investigated and pose no problem for the suggested design.

A separate RF frequency must be synthesized for each antenna beam position. This is the function of the frequency synthesizer shown in Figure I-2. The output of the frequency systhesizer is applied to an injection-locked oscillator to obtain a greater power level. The output of the injection-locked oscillator is then frequency multiplied and applied to the transmitter for the final power amplification. The frequency synthesizer also develops the local oscillator frequencies, offset from the transmitted frequency by the IF frequency to be applied to the mixers.

Assume that the modulator has driven the transmitter to the ON condition. The short pulse burst of RF energy is split with one-half the power being channeled toward each antenna. The duplexer "fires," setting a low impedance in the path to the antenna and a high impedance in the path to the mixer. Thus, the duplexer serves two functions: it protects the mixer during transmission and routes the RF energy to the proper path depending upon the operational mode, i.e., transmit or receive. The isolator between the power splitter and duplexer has a very small RF loss for energy emanating from the RF transmitter, but a very large loss for energy reflected back toward the transmitter. Thus, reflected energy due to mismatches in the RF hardware cannot cause the transmitter to become unstable.

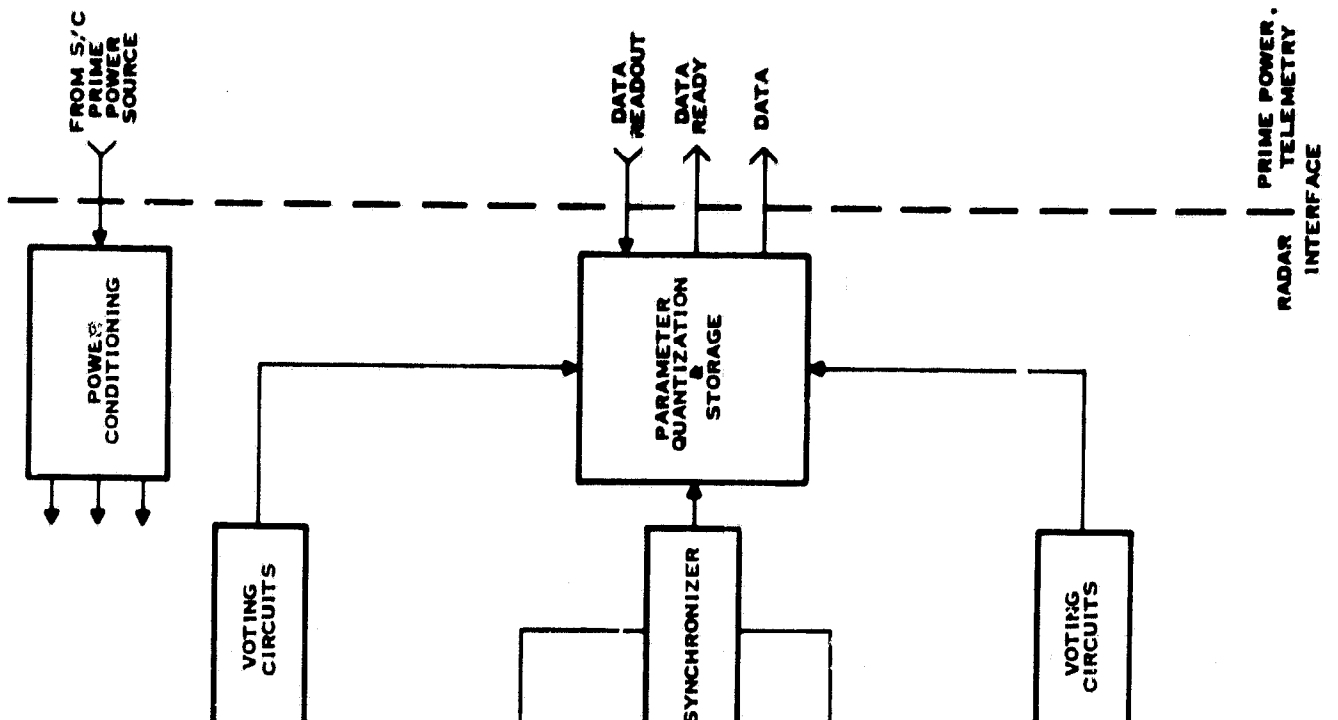


Figure I-2. System Functional Block Diagram

69896

When reflected energy is received from a particle, the duplexer has a low impedance in the antenna-to-mixer path. The return energy is mixed with the local oscillator signal and the lower sideband is amplified and linearly detected by the IF amplifier and detector. This amplifier contains only sufficient power gain to ensure a low system noise figure. The remaining gain is contained in a set of seven video amplifiers. These video amplifiers are in series and their gain is controlled to 2 percent by feedback techniques. This, in conjunction with a calibration signal, gives the maximum accuracy in measurement of the level of the return energy.

The calibration signal is obtained by inserting a small amount of the RF transmitter frequency from the injection-locked oscillator into the RF section via a coupler. This inserted signal is processed through the same circuitry as the return particle energy and will be used to calibrate the system for changes in sensitivity. Such calibration is required for accurately determining the radar cross section of a detected particle.

The output of each of the video amplifiers will go to an identical voting circuit. These circuits choose the amplifier whose output is within specific limits (effective but unsaturated) and pass this output on to the parameter quantizer and storage for further processing. The parameter quantizer, in conjunction with the synchronizer, also determines the two space angles, and radar range to the particle for each detection and the travel time between the two separated beams prior to the second detection. Thus, all parameters needed to characterize the particle will be determined.

The final function to be discussed is the noise automatic gain control (noise agc). The system noise power at the final threshold is a complicated function involving RF losses, temperature, IF bandwidth, and receiver gain. Since these functions will vary considerably over the mission lifetime, a means to control the ratio of detection threshold to noise power is required. This is often called a constant false alarm receiver (cfar). As shown in Figure I-2, the detection threshold is constant and the noise power is adjusted by controlling the gain in the IF amplifier.

## C. SUBSYSTEM DESCRIPTIONS

### 1. Antenna Description

#### a. Requirements

The meteoroid radar system measurement technique uses two pencil beams separated by 10 degrees in a plane normal to the scanned direction. High scan rates are required which will necessitate the use of electronic scan. The system requirements set as a goal the following constraints upon the antanna system.

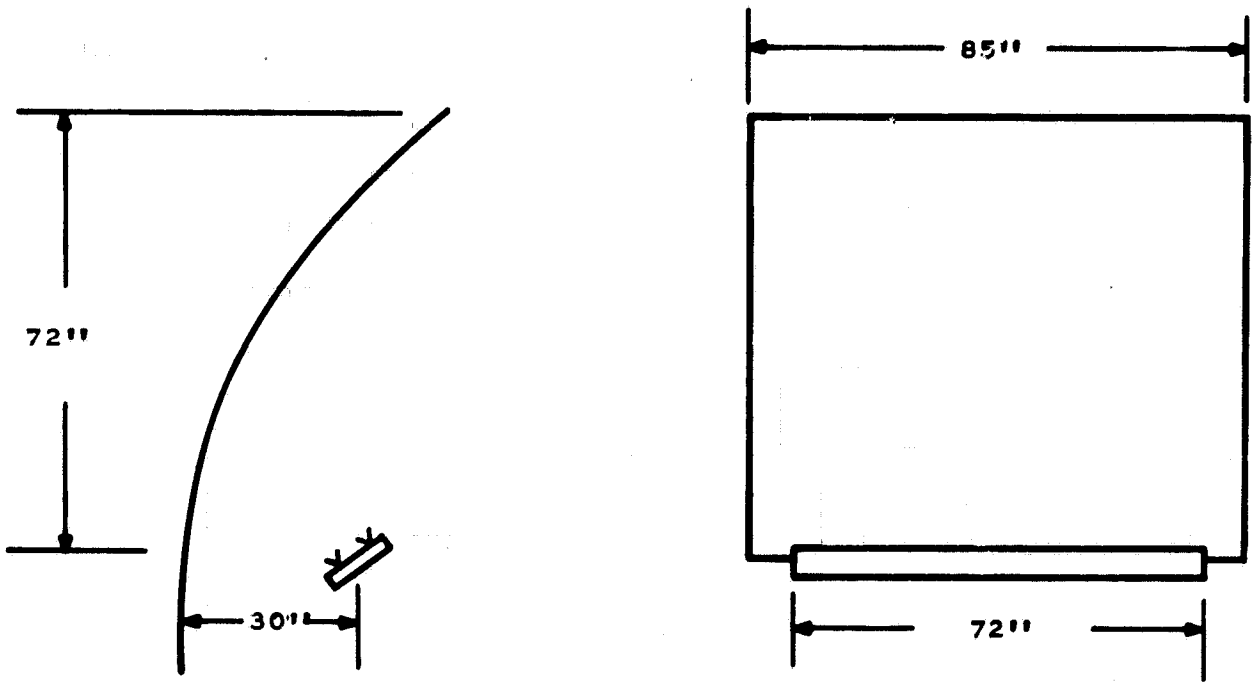


69897

Figure I-3. Offset Fed Cylindrical Parabola

| | |
|---|---|
| Frequency | 15.0 GHz |
| Bandwidth | 0.650 GHz |
| Half Power Beamwidth | 0.5 × 0.5 degree |
| Maximum Scan | ±12.5 degrees |
| Scan Rate | 20 kHz |
| Beam Separation | 10 degrees |

A large physical aperture is required to meet the beamwidth requirements but most vehicles used for this mission necessitate minimizing the launch configuration, i.e., the antenna system must be deployable in space. Another constraint on the antenna is the transmitter; associated equipment must be mounted as near the antenna as possible to eliminate long lengths of transmission line.

The most promising solution to the antenna problem is an offset-fed cylindrical parabola fed by two separated line sources which are electronically scanned. This configuration is illustrated in Figure I-3. An offset feed is chosen so that the feed and part of the reflector can be fixed to the vehicle, thus minimizing deployment problems. The feed system and radar equipment may also be mounted close together.

Following is a discussion of the antenna system design with possible problem areas.

b. Reflector Design

The antenna system will include a cylindrical parabola with an offset feed. Two line sources are offset about the focus of the parabola to give the two displaced pencil beams. The beams are collimated in one plane by the parabola and in the other plane by the line source. The height ($H_R$) of the parabolic section is determined by the desired beamwidth normal to the line source. The length ($L_R$) of the plane section of the reflector will be fixed by the length ($L_A$) of the line source and the maximum scan angle $\theta_m$ as given in the following relation.

$$L_R = L_A + f \tan \theta_m \qquad (1)$$

where

f = focal length.

The height of the reflector was chosen to be 72 inches to give a 0.7-degree half power beamwidth with a 12-dB edge taper. The 12-dB edge illumination was chosen to give maximum gain. The relative reflector-feed positions are illustrated in Figure I-4 for a focal length of 30 inches. As can be seen in the figure, the feed normal does not bisect the reflector included angle of 93 degrees but is skewed upward to give equal edge illumination for the reflector top and bottom.

To obtain the two separated beams, two line sources are displaced from the focus as shown in Figure I-4. The beam offset caused by this feed offset is a function of aperture illumination and f/d ratio. The feed offset angle from the focus ($\Omega_F$) is related to the beam offset from boresight ($\Omega$) by the beam factor (BF) which has been determined empirically.[1] The beam factor for f/d = 0.25 is approximately 0.7 and the beam offset angle is 5 degrees, thus giving the feed offset angle as follows.

$$\Omega = (\Omega_F)\,(BF) \qquad (2)$$

$$\Omega_F = 7.15 \text{ degrees}$$

Thus, the feed offset from the focus (S) is equal to 3.75 inches or the distance between the two feeds (2S) is 7.5 inches. It must be pointed out that this is only an approximate design and that in the actual design a scale model antenna must be constructed and the optimum aperture illumination and feed separation must be determined empirically. Much of the design can be done with computer simulation.

[1] Jasik, H., Antenna Engineering Handbook. 1961, McGraw-Hill, New York, p. 15—21.

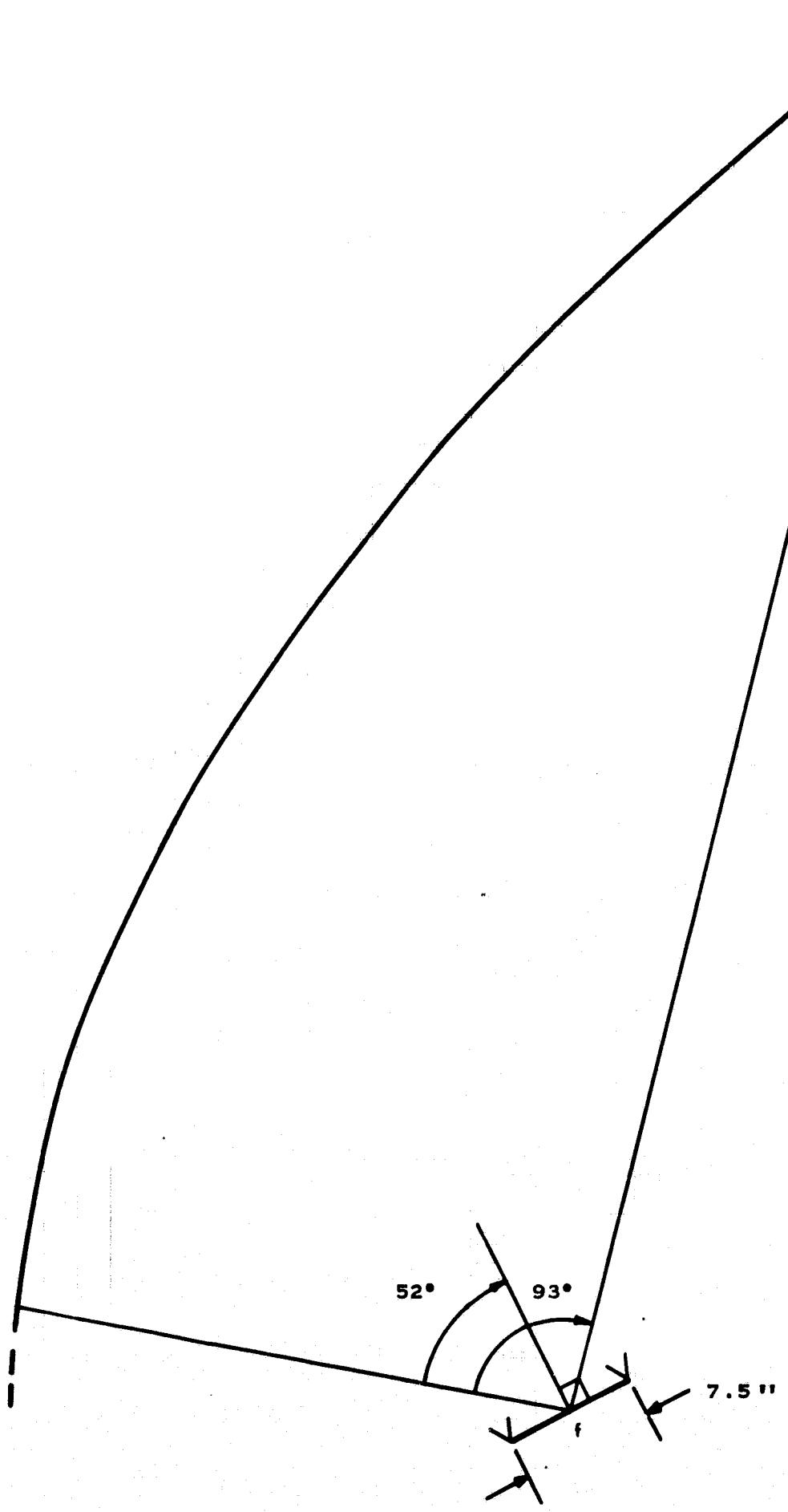


69898

Figure I-4. Relative Reflector Feed Positions

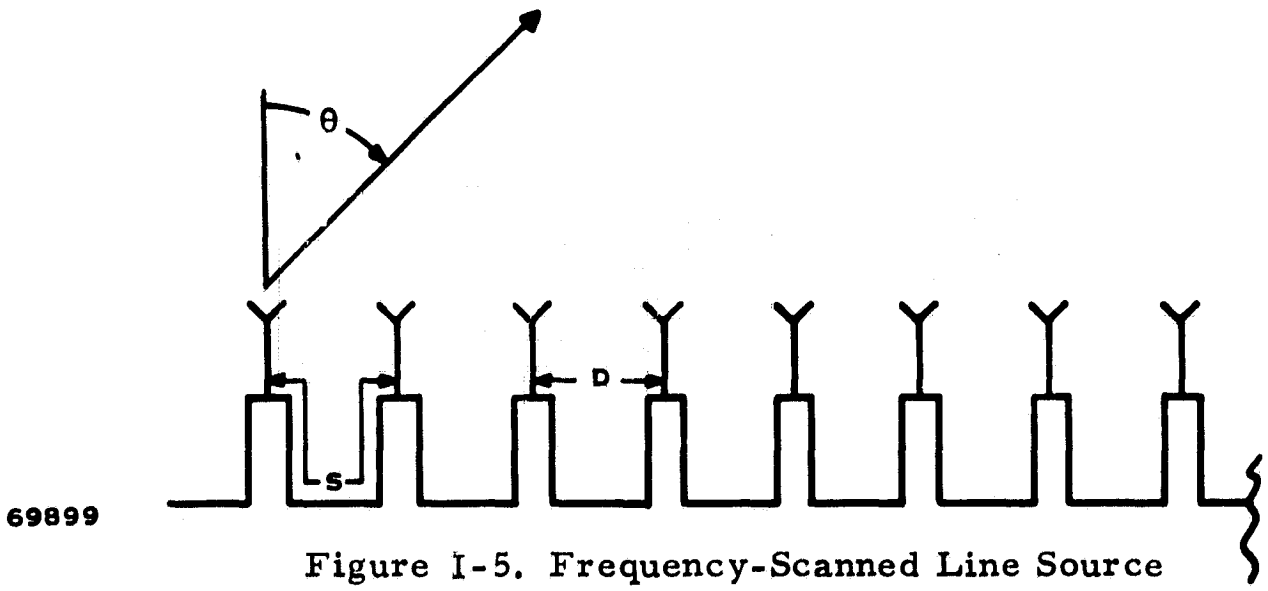


Figure I-5. Frequency-Scanned Line Source

The line source feed aperture must be a 1.0 λ aperture E-plane horn to properly illuminate the reflector. This aperture size gives a 49-degree, 3-dB beamwidth and a 90-degree, 10-dB beamwidth. Thus, the line source aperture height is 0.785 inches.

c. Line Source Feed

The line source is required to scan ±12.5 degrees at a high scan rate for the meteoroid radar application. The small scan angle and high scan rates make a frequency scanned array a desirable choice. The frequency scanned array is a linear array of radiators with a traveling wave feed. Following is a short discussion of the frequency scan theory.[2]

The array space factor as a function of inter-element phase shift $\psi$ is given by

$$S = \sum_{n=1}^{N} A_n \left[\exp jn\,(kd \sin\theta - \psi)\right] \tag{3}$$

for an array as shown in Figure I-5. The array factor will have maxima for $(kd \sin\theta - \psi) = -2m\pi$, where m is an integer. Thus,

$$\psi - 2m\pi = kd \sin\theta \tag{4}$$

where

$$k = 2\pi/\lambda.$$

The array for this application must have only one maximum for the scan volume; thus, $d/\lambda$ must satisfy the following relation.

$$d/\lambda = \frac{1 - 1/n}{1 + \sin\theta_m} \tag{5}$$

[2]Hansen, R. C., Microwave Scanning Antennas, 1966, Academic Press, New York, pp. 135—214.

where

$n$ = number of array elements

$\theta_m$ = maximum scan angle.

For a frequency-scanned array, the phase lag $\psi$ between elements is given by $k_g S$ where $k_S = 2\pi/\lambda_g$ and S is defined in Figure I-5. Feed length S is chosen to satisfy

$$2m\pi = \frac{2\pi S}{\lambda_{go}} \tag{6}$$

to give a broadside maximum at the center frequency $f_o$. The relation between scan angle $\theta_m$ and the frequency is derived as follows:

$$\psi_m = k_{gm} S = \frac{2\pi}{\lambda_{gm}} S \tag{7}$$

where $\lambda_{gm}$ = guide wavelength at $f_m$.

Substituting in Equation (4) gives

$$\frac{2\pi S}{\lambda_{gm}} - 2m\pi = \frac{2\pi d}{\lambda_m} \sin\theta_m \tag{8}$$

and using Equation (6),

$$\frac{2\pi S}{gm} - \frac{2\pi S}{go} = \frac{2\pi d}{m} \sin\theta_m$$

which reduces to the frequency scan equation

$$\frac{1}{d}\left\{\frac{\lambda_m}{\lambda_{gm}} - \frac{\lambda_m}{\lambda_{go}}\right\} = \sin\theta_m \tag{9}$$

where S/d is commonly referred to as the "wrap up" ratio.

A section view of the frequency-scanned feed is shown in Figure I-6a. Slots are cut into the waveguide broadwall to form radiators and a horn is formed above and below the slots to properly illuminate the reflector. The horn in this case is an H-plane horn with an aperture dimension of $1.4\lambda$(1.1 inch) to give a 12-dB edge taper. The two feeds are placed side-by-side as shown in Figure I-6b to give the displaced beams.

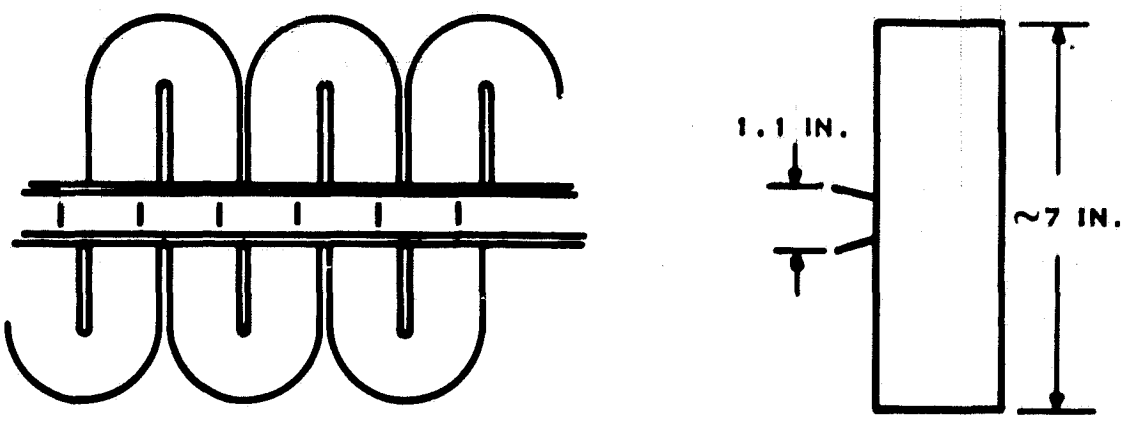


(a) FREQUENCY SCANNED SOURCE

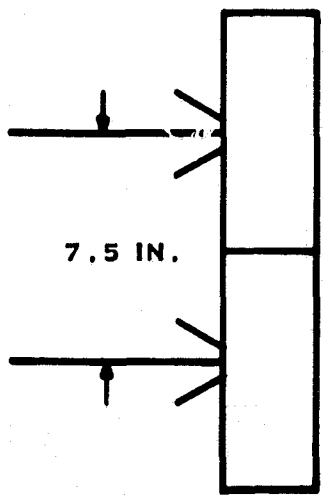


(b) STACKED FEEDS

69900

Figure I-6. Feed Structure Geometry

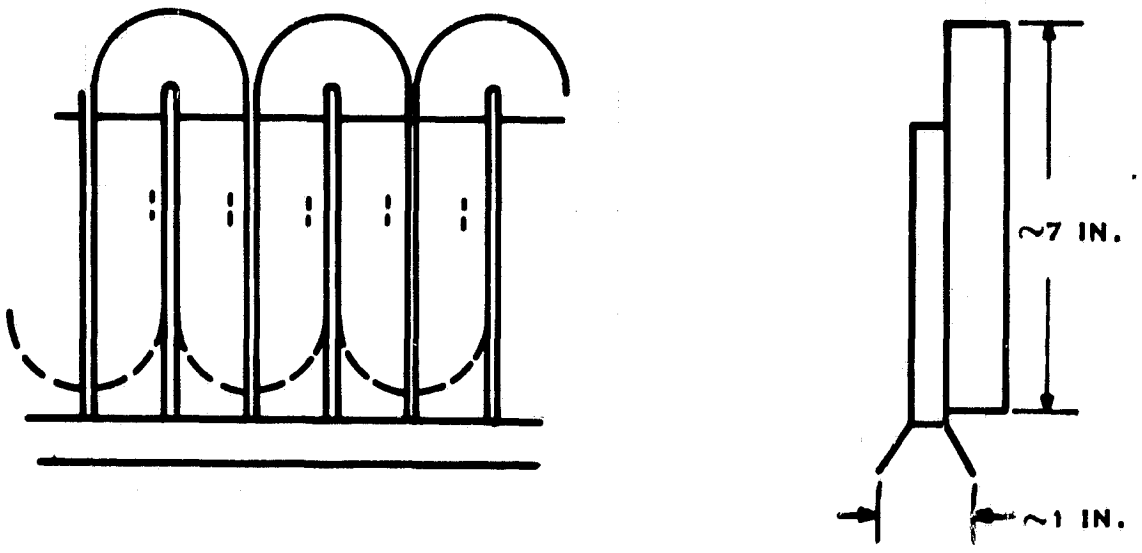


69668

Figure I-7. Alternative Frequency-Scanned Source Geometry

On alternate technique for forming the radiator is shown in Figure I-7. The slots in the frequency scan feed excite waveguides which are terminated in the horn. This method will give a lower feed profile which is desirable if the horn spacing is less than the frequency scan feed height. The parameters for the frequency-scanned array, assuming the first feed structure, are given in Table I-1.

Table I-1. Array Feed Structure Specifications

| | |
|---|---|
| Frequency | 15.0 ±0.325 GHz |
| Array Length | 72 inches |
| Radiator Spacing | $0.8\lambda_o$ (0.629 inch) |
| Number of Radiators | 114 |
| Feed Waveguide | RG-107/U (WR 62) Aluminum |
| Feed Length | 7.11 inches (Interelement) |
| Attenuation | ~0.06 dB/foot |
| Weight | ~0.097 pound/foot |
| Total Feed Length | ~68 feet |
| Maximum Scan | 13.7 degrees (15.325 GHz) |

d. Antenna System

The size of the reflector necessitates the deployment of the antenna in space. The $K_u$-band frequency severely limits the amount of packaging possible with the antenna because small tolerances must be held to give good radiation patterns. Poor deployment will cause loss in directivity, increased sidelobes, and pointing error. The assembly of the frequency scan feeds is particularly critical to maintain accurate scan characteristics and to have the two beams scan together.

The reflector may be inflatable or extendable. An inflatable reflector antenna at $K_u$-band does not seem practical because reflector surface accuracy must be good to give acceptable performance. The extendable reflector is possible if the number of parts to be unfolded or extended are held to a minimum and the extending operation can be accomplished precisely. Several views of such an antenna are shown in Figures I-8, I-9, and I-10 in both stowed and extended positions.

The meteoroid antenna characteristics are given in Table I-2.

Table I-2. Antenna System Characteristics

| | |
|---|---|
| Frequency | 15.0 ±0.325 GHz |
| Scan | ±13.7 degrees |
| Beamwidths | 0.7 by 0.6 degrees (0.6° in Scan Plane) |
| Beam Separation | 10 degrees |
| Reflector Dimensions | 72 by 85 inches |
| Array Dimensions | 72 by 14 by 4 inches |
| Focal Length | 30 inches |

The reflector will be constructed of epoxyglass honeycomb material. Its reflector surface is sprayed with a metallized compound that gives the desired reflector properties, including close control of mechanical tolerances.

A complex deploying mechanism is required to erect the large aperture antenna on a spacecraft the size of the Mariner '69. Manufacturing tolerances must be controlled very closely on the reflector and feed. Additionally, the reflector and feed relationship must be accurately positioned. The offset-fed cylindrical parabola, shown mounted to a Mariner '69 size spacecraft in Figure I-11, is an approach that will fulfill the imposed requirements.

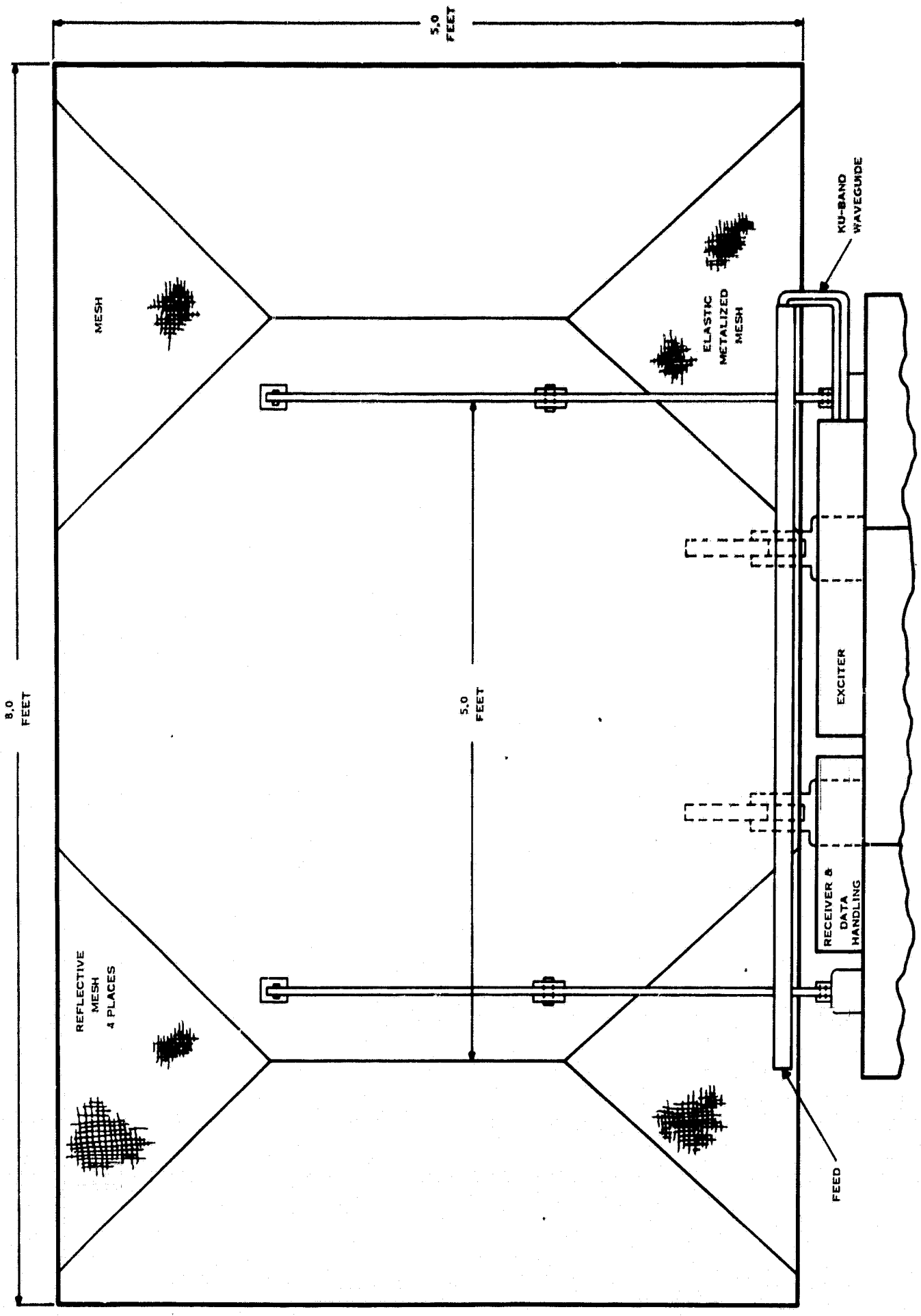


Figure I-8. Antenna Front View—Deployed

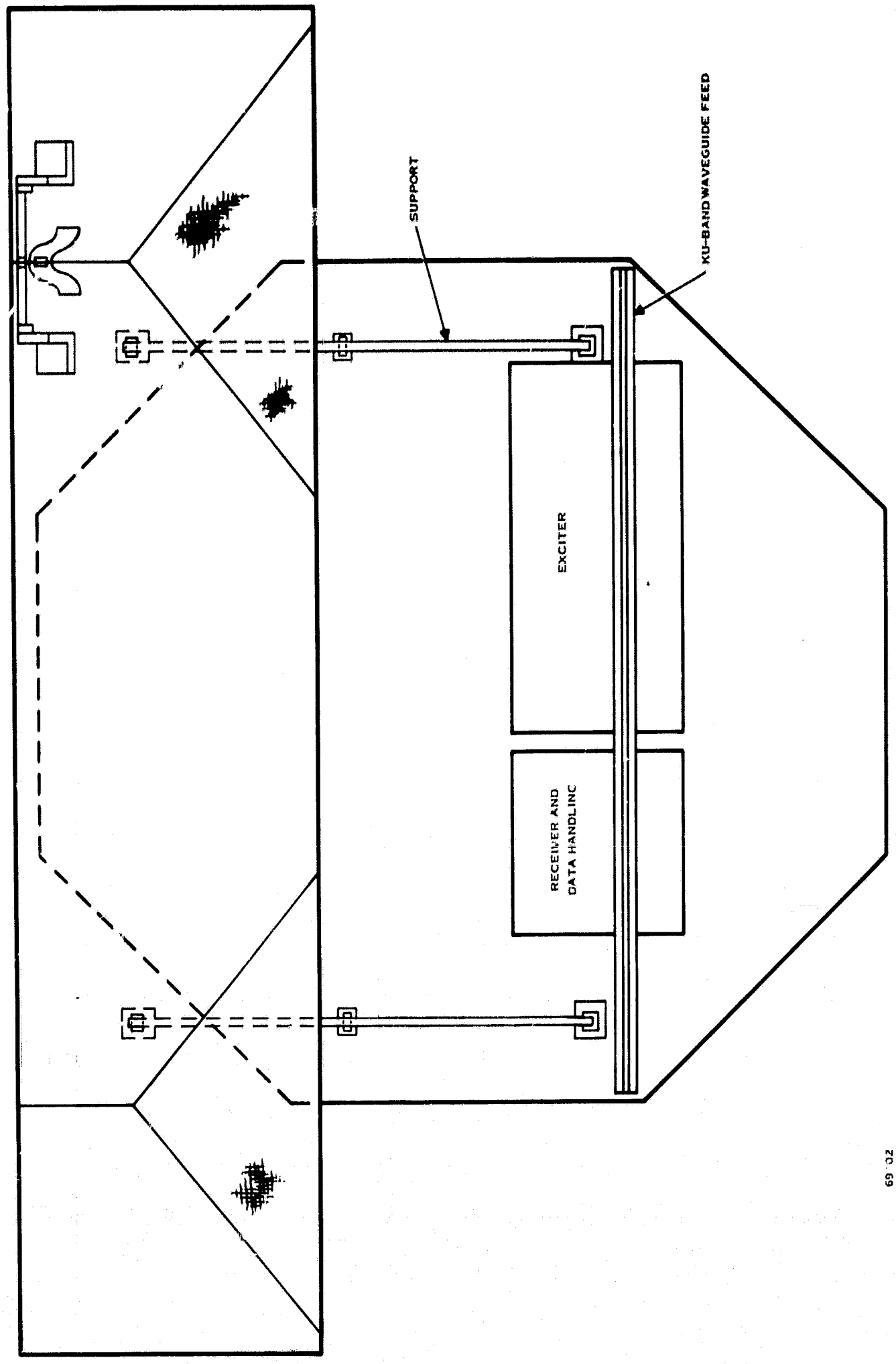


Figure I-9. Antenna Top View—Deployed

69-02

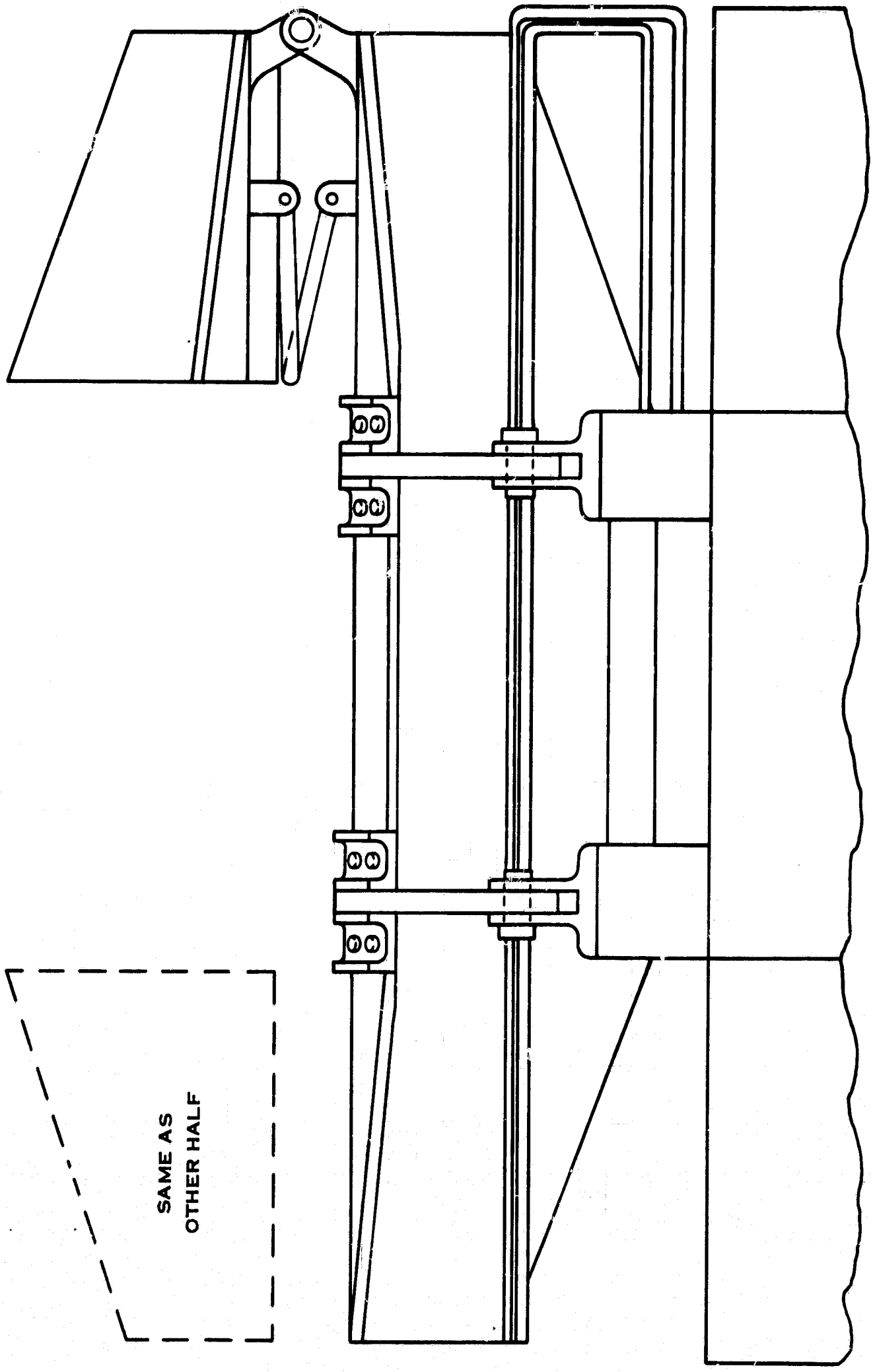


Figure I-10. Antenna Rear View—Stowed

69701

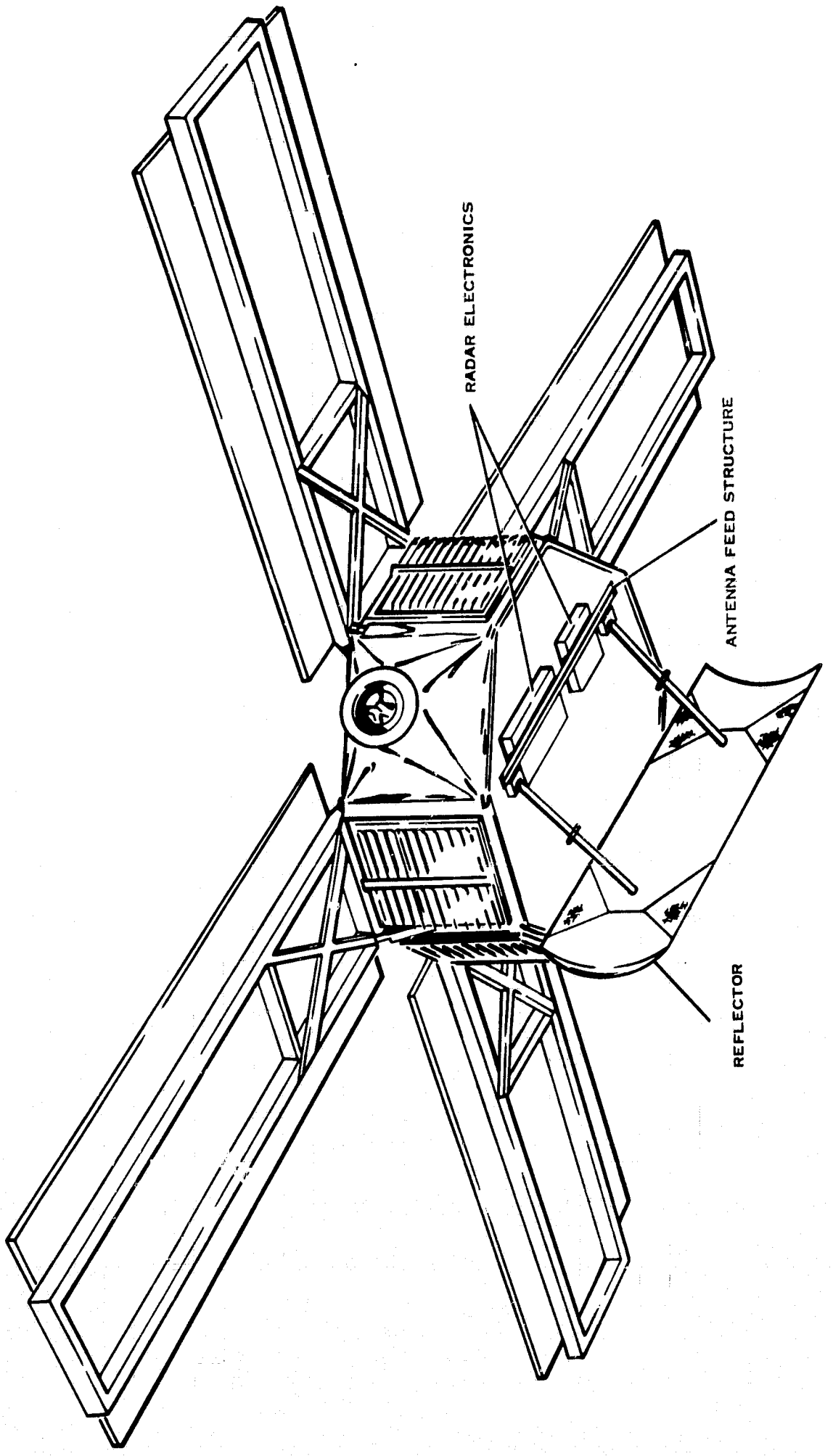


Figure I-11. Antenna Mounted on a Mariner '69 Type Spacecraft

As shown in the figure, the feed is fixed permanently to the spacecraft substructure. In the launch condition, the two outer portions of the antenna fold behind the antenna so that the antenna outline matches the spacecraft outline. The antenna then folds onto the spacecraft face and is rigidized. Antenna deployment is accomplished in the reverse manner.

2. Frequency Synthesizer Description

The frequency synthesizer consists of three separate but essentially identical subfrequency synthesizers with frequency outputs in the 200-MHz range. Two of these are used alternately to provide the receiver local oscillator frequency and the third is used to provide the transmitted frequency. With reference to Figure I-12, the 200-MHz signals are mixed with a 1.8-GHz signal and the upper sideband is selected with a bandpass filter (BPF). This upper sideband is then frequency multiplied by eight to obtain the desired RF frequencies for the transmitter and receiver.

The subfrequency synthesizers must supply any one of 50 different frequencies uniformly spaced at 1.2-MHz intervals across a band with an approximate center frequency of 200 MHz (212 MHz for the transmitter channel). This is accomplished with the sampled-data phase-lock loop system shown schematically in Figure I-13.

This system will seek a state in which the sample pulse occurs at the same portion of the reference sawtooth waveform during each cycle of the reference signal. In this state, the frequency of the sample pulse must be the same as that of the reference signal. Thus, the frequency of the voltage controlled oscillator (VCO) must be exactly N times the frequency of the reference signal. Any tendency for the VCO output frequency to change from this value will cause a movement of the sample pulse relative to the reference signal. This will result in a change in the level of the signal controlling the VCO, which will correct the error in frequency.

The steady-state accuracy of the synthesizer output frequency is the same as the accuracy of the reference oscillator. Simple crystal oscillators are available with an accuracy of five parts in $10^5$ over a wide temperature range. This would give an accuracy in the relative spacing of the beams several orders of magnitude better than required.

With the configuration specified as in Figure I-13, the important parameters to be chosen are the VCO sensitivity or "gain" and the configuration of the filter. These must be selected to meet the requirements for (1) spectral purity of the VCO output, and (2) an acceptable loop when a new frequency is requested (i.e., when N is changed to a different number) by the control logic. The following parameters will be shown to yield acceptable system performance.

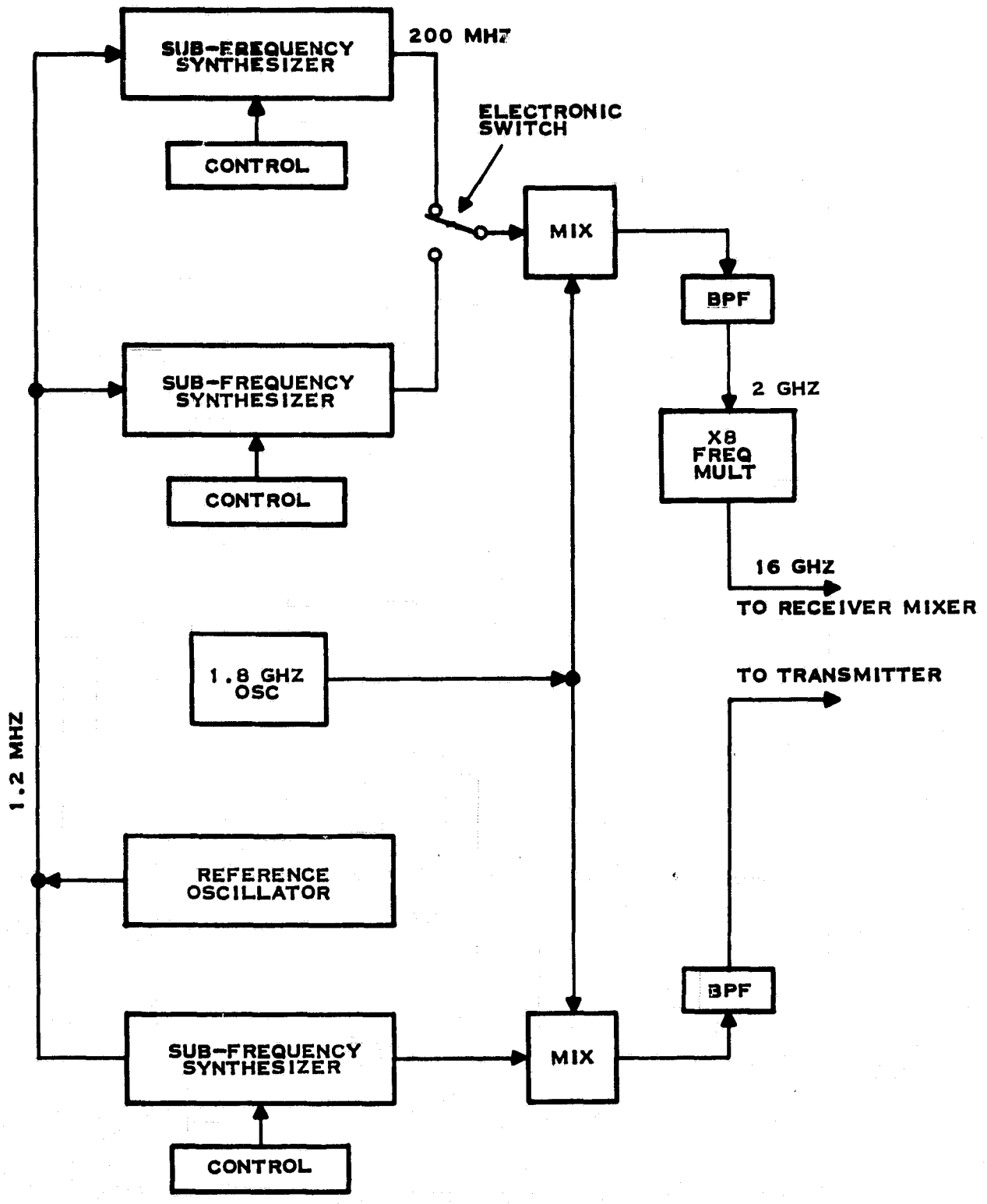


69669

Figure I-12. Frequency Synthesizer

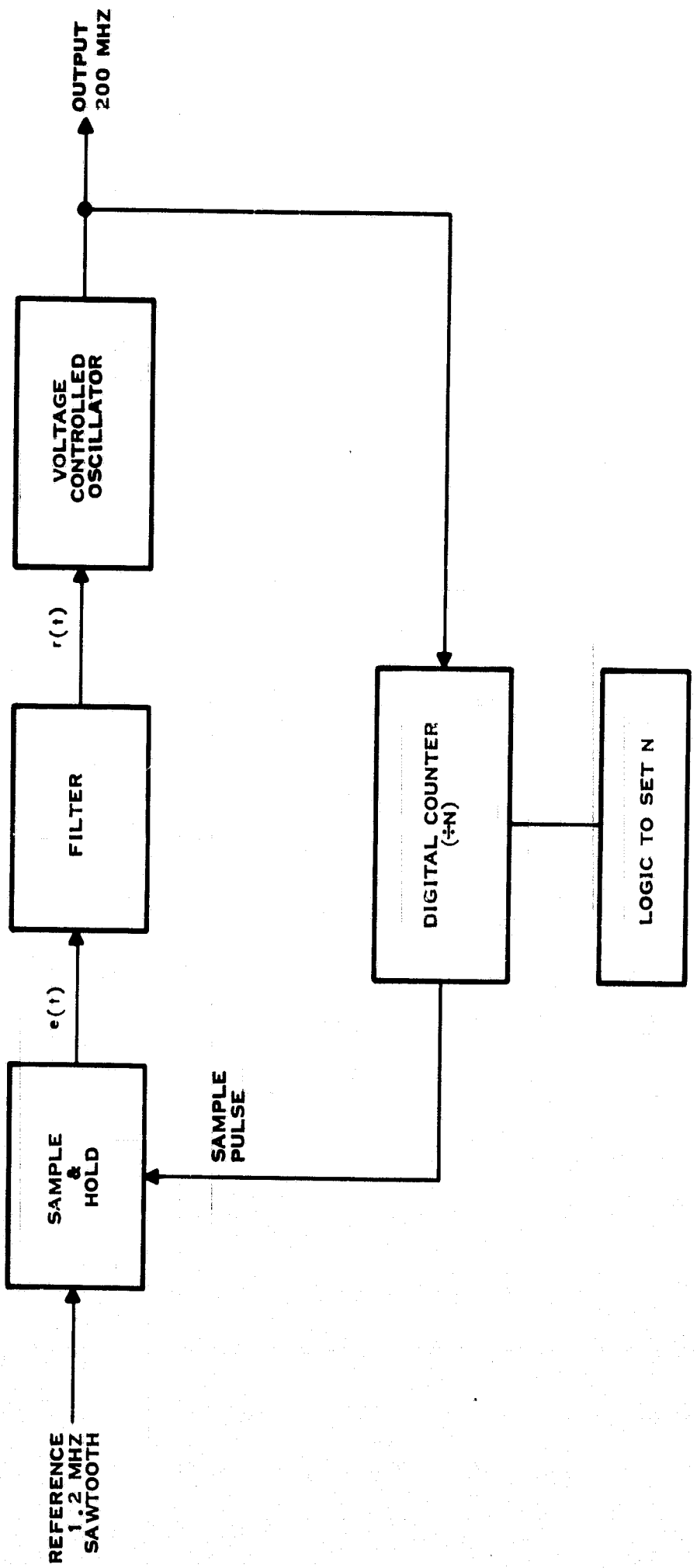


Figure 1-13. Sampled-Data Phase Lock Loop

69670

VCO Sensitivity: $1.2 \times 10^8 \frac{\text{radian}}{\text{volt} \cdot \text{sec}}$

Filter transfer function: $H(s) = \frac{1}{(1.04 \times 10^{-6} s + 1)^3}$

Sample-and-hold circuit gain: $1 \frac{\text{volt}}{\text{radian}}$

For the above value of VCO sensitivity, the phase error will normally be limited to a range of $\pi$ radians for the desired VCO frequency range of 60 MHz. This allows an additional variation of $\pm\pi/2$ radians to correct for drift and inaccuracies in bias levels and oscillator center frequency.

Frequency components of the phase detector output signal occurring at multiples of the reference (sampling) frequency, and which are not removed by the filter, will modulate the VCO, creating sidebands around the desired oscillator frequency output. These sidebands must be attenuated to attain satisfactory spectral purity. Since a low-pass filter will be used and the modulation constants will be small, it is only necessary to consider the sidebands nearest the oscillator frequency. These sidebands are caused by components of the phase detector signal and are separated from the desired signal by the reference frequency. All other sidebands will be smaller than the nearest sidebands.

A reasonable sample-and-hold circuit will operate satisfactorily with a sample pulse no wider than 10 percent of the period of the reference signal. If this ratio is 10 percent and the sampling interval does not include the flyback section of the sawtooth, the component of the phase detector output at the reference frequency will have a magnitude

$$C_1 = \left| \frac{1}{\pi} \int_{-\frac{\pi}{5}}^{0} -t \exp(jt) dt \right| = 0.621$$

and the same component of the filter output will have a magnitude

$$r_1 = |H(j \omega_r)| \cdot C_1$$

where $\omega_r$ is the reference frequency.

If the gain of the VCO is $k_o \frac{\text{radian}}{\text{sec} \cdot \text{volt}}$ and the magnitude of the desired output component is assumed to be unity, the magnitude of the first sidebands is

$$s_1 = J_1\left[\frac{k_o r_1}{\omega_r}\right]$$

when $J_1(\cdot)$ is the Bessel function of first order and first kind. For small values of the argument, this is approximately

$$s_1 = \frac{k_o r_1}{2 \omega_r}$$

If the sidebands are required to be 40 dB below the desired component, and the gain parameters are as given previously,

$$H(\omega_r) = \frac{2 \omega_r s_1}{c_1 k_o} = 0.00202$$

This requirement can be met with a filter of the form

$$H(s) = 1/(\tau_3 s + 1)^3$$

where

$$\tau_3/T = 1.25$$

and T is the period of the reference signal.

The characteristics of the above filter will, to a large extent, determine the acquisition times and resulting frequency error. Straightforward analysis of the system with a third-order filter requires deriving and finding the roots of a fourth-order characteristic equation. However, this filter can be approximated by one of a lower order, greatly reducing the difficulty of the analysis. As will be shown later, the value of the parameter $k_o T/N$, which is roughly analogous to the open-loop gain for a continuous system, is on the order of 0.5 so that there is never any problem of stability with this system, and the differences in the phase characteristics of the third-order filter and its approximation do not introduce appreciable error. For this analysis, the third-order low-pass filter will be approximated by a first-order low-pass filter that has the same energy in its impulse response. This filter has the transfer function

$$H_a(s) = \frac{1}{(\tau s + 1)}$$

where

$$\tau/T = \frac{8}{3}(\tau_3/T) = 3.33$$

Thus, the system is approximated by one with an open-loop transfer function of

$$\frac{k[1 - \exp(-Ts)]}{s^2(\tau s + 1)}$$

whose partial fraction expansion is

$$k\left[1 - \exp\left(-Ts\right)\right]\left[\frac{\tau}{s^2} + \frac{\tau^2}{z - \exp(-T/\tau)}\right]$$

where

$$k = k_o/N.$$

The corresponding z-transformed transfer function is

$$k(z-1)\left[\frac{T}{(z-1)^2} - \frac{\tau}{z-1} + \frac{\tau}{z - \exp(-T/\tau)}\right]$$

Thus, the characteristic equation is

$$0 = z^2 + z\left[-\exp(-T/\tau) - 1 + kT - k\tau + k\tau\exp(-T/\tau)\right]$$
$$+ \exp(-T/\tau) - kT\exp(-T/\tau) + k\tau - k\tau\exp(-T/\tau)$$

For the system specified,

$$kT = \frac{k_o T}{N} = \frac{(1.2 \times 10^8)(1.2)}{(1.2 \times 10^6)(200)} = 0.6$$

For these values of kT and $\tau/T$, the roots of the characteristic equation are

$$z = 0.830 \pm j0.356$$

The magnitude of these roots is 0.9026. Thus, the frequency error of the system n samples after a command to change frequency by an amount $\Delta f$ will be

$$\Delta f(0.9026)^n$$

where $\Delta f$ is the difference between the old frequency and the new frequency. For the transmitter, $\Delta f$ (after the X8 frequency multiplication) is 10 MHz. If the prf is set at 20 kHz, the interval between transmitter pulses will contain approximately 60 samples, and thus

$$e_f \leq 10^7 (0.9026)^{60} < 22 \text{ kHz}$$

Since the IF bandwidth is 2.2 MHz and the doppler shift due to relative motion of the target may be as large as 100 kHz, this is an acceptable error.

If the prf is reduced to 10 kHz, this performance can be obtained with a second-order filter. The use of a sample pulse narrower than 10 percent of the period of the reference will also loosen the restrictions on the filter. The frequency error ($e_f$) for the local oscillator frequency will be twice as large because the two subsynthesizers alternate and must have twice the frequency shift in the same length of time. The error is quite small and will not degrade the system performance.

A schematic diagram of the divider and its control logic is illustrated in Figure I-14. The simplest way to implement the divider is to use a ripple-through counter. The counter is reset to $\bar{N}$, the one's complement of N, and an AND gate is used to sense the "all ones" state and reset the counter again.

A sample pulse can easily be generated from this counter with another AND gate. A four-input gate connected to the four highest-order stages of the digital divider will produce a pulse of width $16/f_{out}$. For $f_{out}$ = 200 MHz, this is a width of 90 nanoseconds. Note that this pulsewidth will vary as the output frequency varies, but that its short-term stability will be much better than that obtained by other methods. This is important since it is the timing of the trailing edge of the sample pulse which is critical in this system.

Thus, the control logic must supply the one's complement of three different values of N simultaneously (one for each frequency synthesizer). This can be done with three independent counters which are incremented at the end of the transmitted pulse so as to progressively step through the band of frequencies required. After the beam scan has been completed, the three counters are reset to the values appropriate to beginning the next beam scan. Since the two receiver subsynthesizers must change alternately, the most significant digit of their respective reset circuits would be connected permanently to the proper value.

Note also that since the frequency change at the end of a beam scan is 50 times greater than that for each step of the beam scan, it may be necessary to allow the synthesizers a longer time to acquire the new frequencies. The transmitter control could easily be designed to skip a beat before starting a new scan.

The absolute accuracy of the beam pointing is largely dependent on the accuracy of the 1.8-GHz oscillator. If the beams are to be correctly aligned to within 5 percent of a beam step, the final output frequency must be accurate to within 5 percent of the size of one frequency step. In the

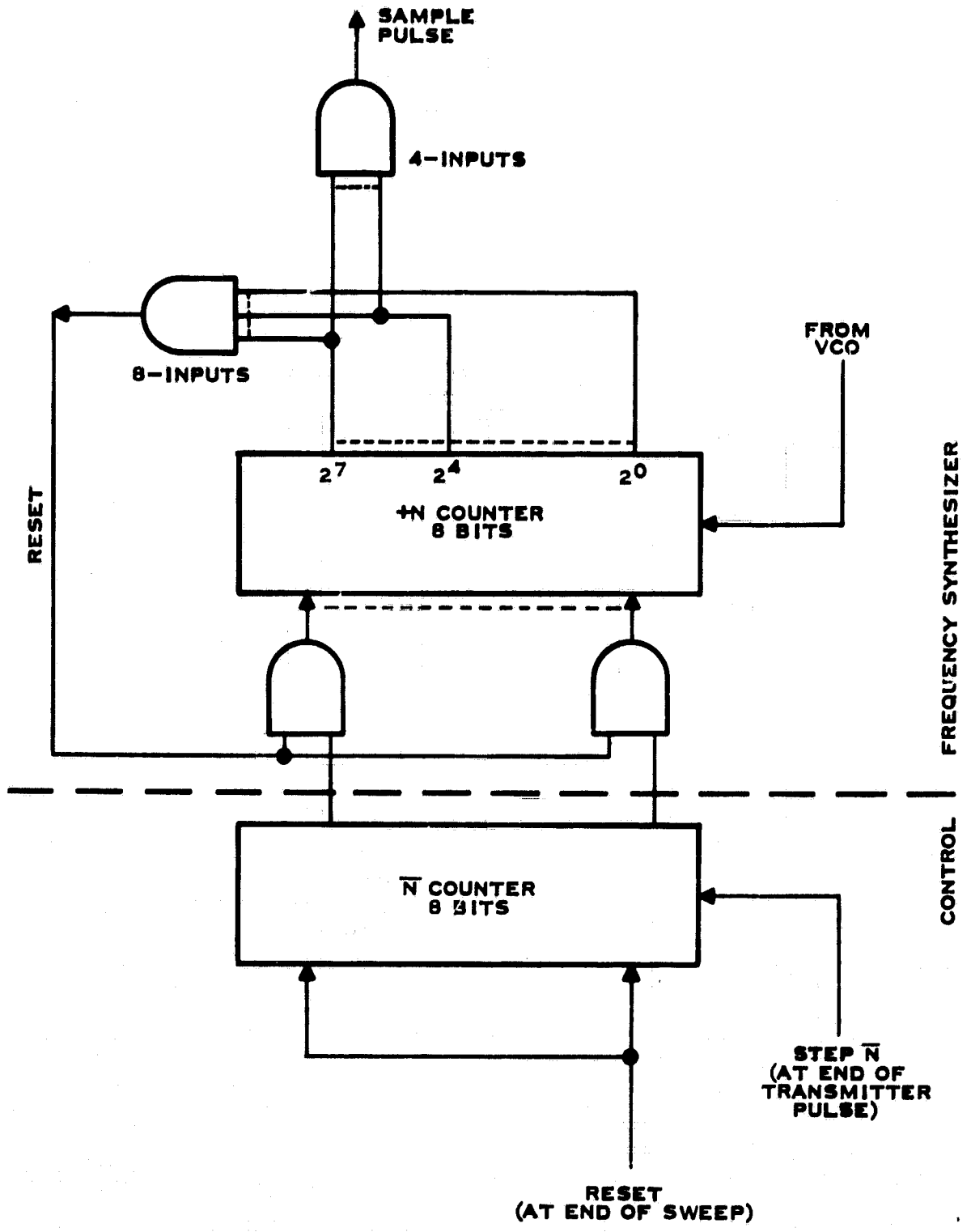


69671

Figure I-14. Frequency Synthesizer Divider and Control Circuit

case of 10-MHz frequency steps, this implies a frequency error of 0.5 MHz or 0.003 percent of the output frequency. Crystal oscillators with this accuracy are available in the 200-MHz region. Such a 200-MHz oscillator followed by a X8 frequency multiplication would meet the requirements.

3. RF Transmitter and RF and IF Receiver Description

The selected configuration for the RF transmitter and the RF and IF receivers is illustrated by Figure I-15. Due to the need for a 10-percent instantaneous RF bandwidth for frequency scanning the antenna beam, a traveling wave tube (TWT) was chosen for the high-power transmitter.

The TWT will be operated as a depressed collector pulse amplifier with grid modulation. The inherent large instantaneous RF bandwidth of the TWT permits more than sufficient turn-on and turn-off speeds to allow pulse modulation through grid control.

The total cathode current splits between the slow wave structure (helix) and collector with less than 10 percent of the total cathode current flowing to the helix. Since the helix-to-cathode voltage determines the tube operation and the collector-to-cathode voltage acts only as an excess electron collector, only the cathode voltage need be regulated precisely.

By supplying a voltage bias to the collector rather than grounding, reduce power dissipation within the tube is realized. The dissipated power transferred to the collector supply can be absorbed more easily and the heat generated can be more readily channeled to a heatsink.

Since the TWT is grid modulated, the RF drive to the TWT is CW. This basic continuous wave is received from the frequency synthesizer at very low power. This wave is used to injection lock an oscillator to increase the available power to drive the TWT. The injection-locked oscillator output is then frequency multiplied by eight and applied to the grid of the TWT. The TWT must have a frequency output at 15 GHz ±10 percent and a peak power of 5 kW. A possible tube for this application is the Hughes 820H.

The power emitted by the TWT is split by a short-slot hybrid with one-half the power being channeled toward each antenna. Two 20-dB finite isolators reduce the reflected power from the duplexer-antenna circuit. Due to the frequency diversity, a mismatch of 2:1 can be expected from the antennas. If this were coupled directly to the TWT, it would seriously degrade its operation.

The duplexer serves two functions. When the tube is transmitting it sets a low impedance in the isolator-to-antenna path and a high impedance in the antenna-to-mixer path, hence protecting the mixer crystals during

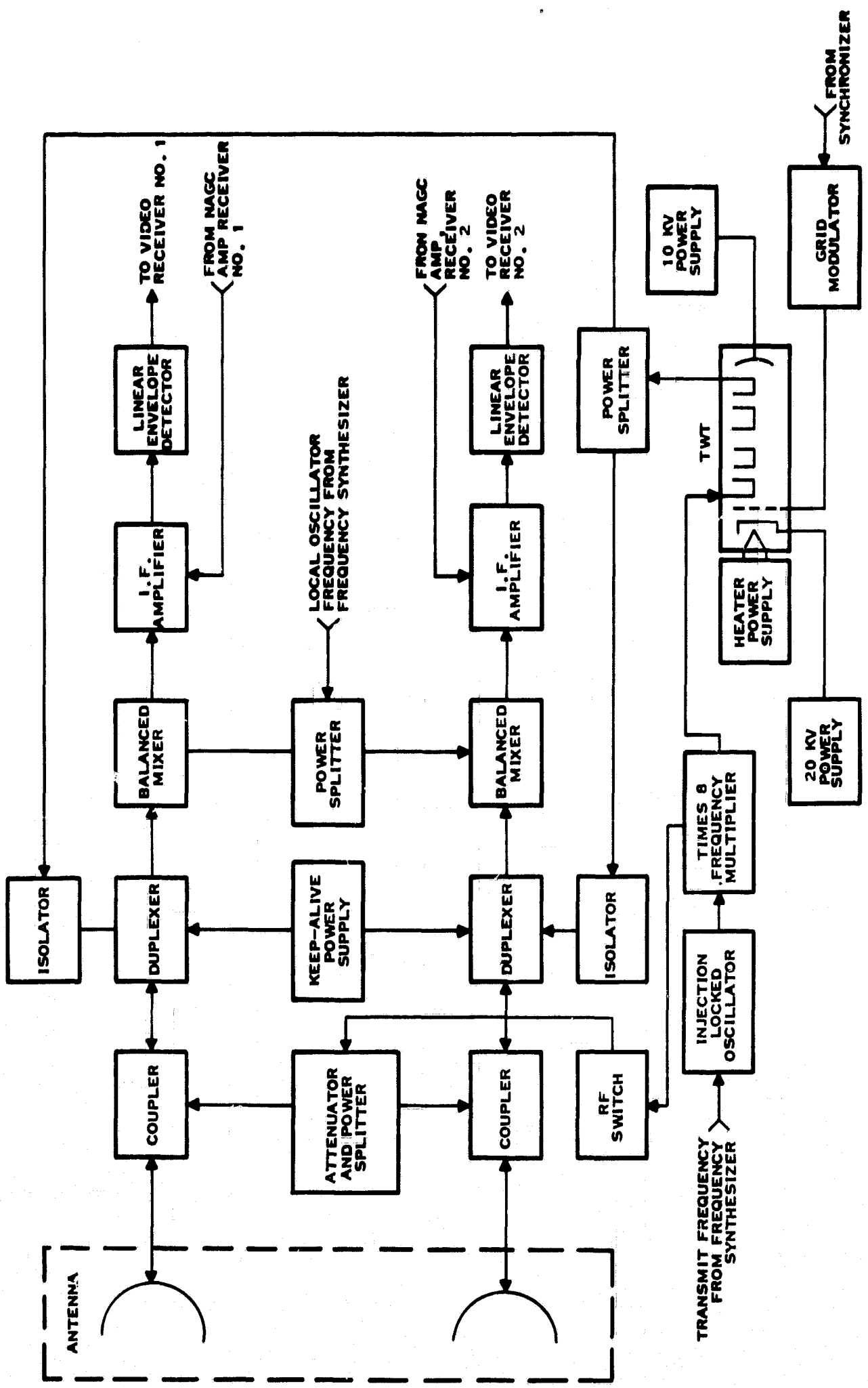


Figure I-15. RF Transmitter and the RF and IF Receivers

RF transmission. When the tube is not transmitting, the duplexer sets a low impedance in the antenna-to-mixer path, thus assuring a minimum RF loss and maximum system sensitivity.

The receiver gain calibration is also in the RF portion. The output of the injection-locked oscillator is coupled into the receive RF path via an RF switch, an attenuator, a power splitter, and an RF coupler. This is intended as a commanded function to be used to check for proper system operation and to calibrate the system for each detected particle. This will calibrate all functions of the system with the exception of antenna gain and the power gain of the TWT. However, the antenna gain will remain very nearly constant and other means can be used to detect changes in the TWT output power which will be discussed later.

The remainder of the RF and IF receiver is conventional. The balanced mixer output is at the IF frequency. The IF amplifier must be linear for a large change in input signal level if the particle cross-section measurement is to be accurate. This also necessitates the use of a linear envelope detector.

4. Video Receiver Description

The receiver will consist of two units: one at an intermediate frequency and one at the video frequencies. The gain in the receiver must be precisely controlled and known, and must also be linear if a good estimate of the particle cross section is to be obtained. The calibration signal that is inserted in the RF section can calibrate the system over a narrow range, assuming that it is a single amplitude signal. Thus, the relative gain between the calibrated signal point and other amplitude measuring points in the system must be held constant and known.

This can most readily be accomplished by the use of negative feedback. However, negative feedback for gain stabilization cannot easily be implemented at the intermediate frequency. It can easily be realized at the video frequencies and with much more efficient use of the available power. For this reason the IF portion of the receiver will have only sufficient power gain to assure an acceptable system noise figure and voltage gain to amplify the maximum received signal to approximately two volts. The remaining gain required will be shared by several stages in the video portion of the receiver. The number of video amplifiers required will depend on the dynamic signal range and the acceptable gain per stage. This, in turn, depends upon the useful, linear, dynamic output swing of the video amplifiers.

One concept for mechanizing the video receiver amplifier chain and the video receiver voting circuits is shown in block diagram form by Figure I-16. The number of identical voting circuit channels is equivalent to the number of identical cascaded video amplifiers. This number will now be determined.

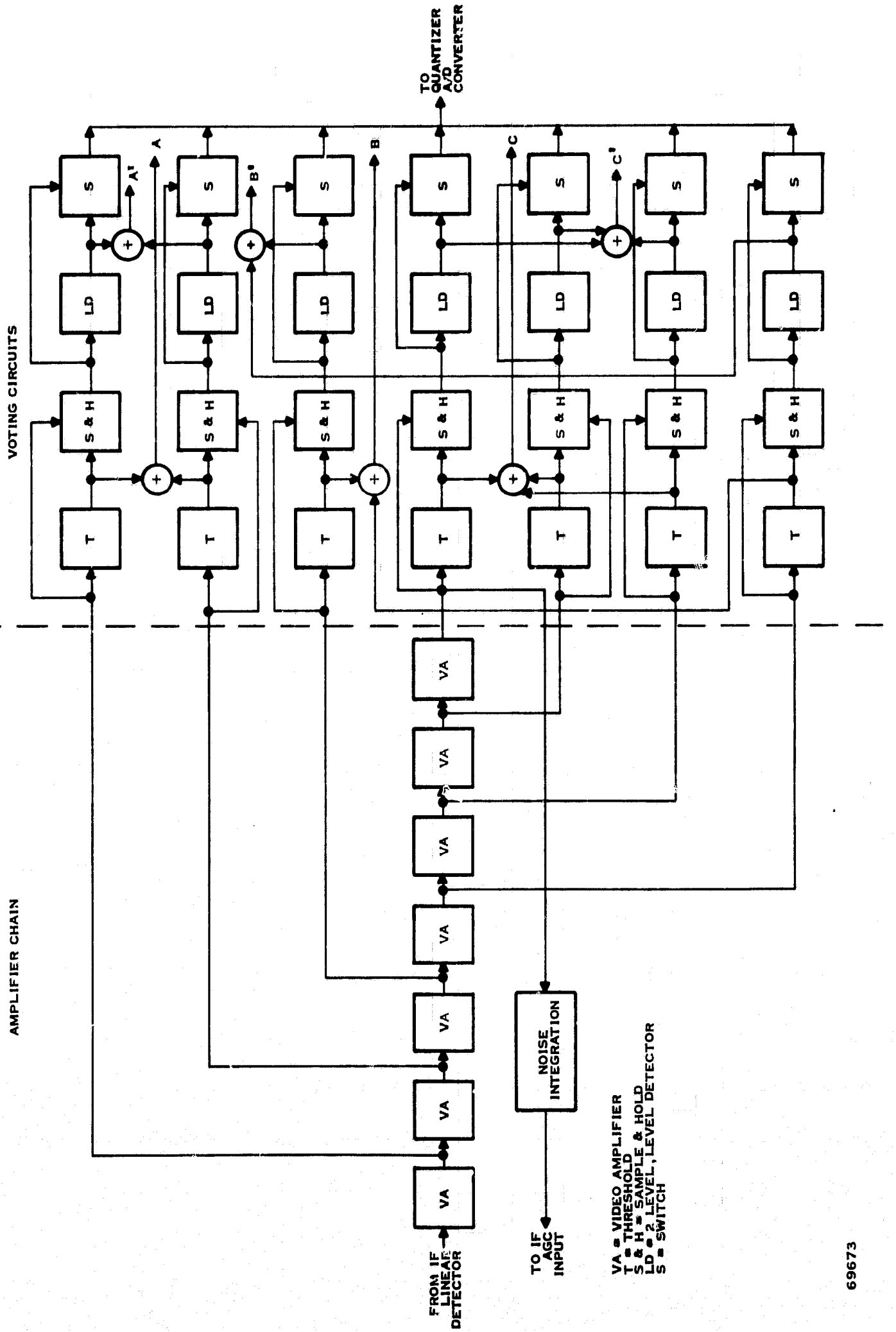


Figure I-16. Video Receiver (Two Required Per System)

The basic system parameters for an optimum design were shown in previous sections to be

minimum power signal-to-noise ratio = S/N
= 16.25 dB = 42.2

dynamic signal range = DR = 50 dB = $1 \times 10^5$

IF noise bandwidth = $B_{if}$ = 2.2 MHz

system noise figure = $\overline{NF}$ = 10 dB = 10.

Thus, the equivalent input noise power is

$$N_o = KT_oB_{if}\,\overline{NF}$$
$$N_o = (1.38 \times 10^{-23} \text{ joule/degree} \times 290°K \times 2.2 \text{ MHz} \times 10)$$
$$N_o = 8.8 \times 10^{-14} \text{ watts}$$

and the minimum signal power ($P_o$) is

$$P_o = N_o(S_o/N_o)$$
$$P_o = 3.713 \times 10^{-12} \text{ watts}$$

The maximum signal power is

$$P_{mx} = P_o\,\overline{DR} = 3.7 \times 10^{-7} \text{ watt}$$

The maximum signal voltage (assuming 100-ohm crystals) is

$$E_{mx} = \left[50(3.7 \times 10^{-7})\right]^{1/2} = 4.3 \times 10^{-3} \text{ volt}$$

Thus, the voltage gain required of the IF receiver is found to be

$$G_{vif} = 2.0/(4.3 \times 10^{-3}) = 465 \text{ volts/volt} = 54 \text{ dB}_v$$

However, since the noise automatic gain control must automatically adjust the system gain to compensate for sensitivity changes, a reserve gain of 6 dB will be included. This makes the total IF voltage gain equal to 60 $dB_v$. Thus, the automatic gain control must have a total range of 12 dB where one-half of this is for reserve operation.

The minimum signal at the IF output detector will be

$$E_{min} = 50(3.73 \times 10^{-12})^{1/2}\,(465) = 6.35 \times 10^{-3} \text{ volt}$$

Hence, for a video threshold input pulse amplitude of 10 volts, which is approximately the limit of linear operation for present day operational amplifiers, the video gain must be

$$G_{vv} = \frac{10}{6.35 \times 10^{3}} = 1.57 \times 10^{3} \text{ volts/volt} = 63.9 \text{ dB}_{v} \text{ (maximum)}$$

$$G_{vv} = \frac{10}{2} = 5 \text{ volts/volt} = 14.0 \text{ dB}_{v} \text{ (minimum)}$$

Thus, the first stage in the video amplifier chain will have a voltage gain of 5 volts/volts. The remaining stages will have a combined gain of 314 volts/volt. Table I-3 shows the gain per stage as a function of the number of stages. Skolnik shows that the detection threshold ($V_t$) is related to the rms noise voltage ($\Psi_o$), the IF bandwidth ($B_{if}$), and the false alarm time ($T_{fa}$) by the relationship

$$T_{fa} = \frac{1}{B_{if}} \exp \frac{V_T^{2}}{2\Psi_o}$$

Table I-3. Possible Gain Per Stage (Total Gain is 314 Volts/Volt)

| Number of Stages | Voltage Gain Per Stage |
|---|---|
| 4 | 4.21 |
| 5 | 3.16 |
| 6 | 2.61 |
| 7 | 2.27 |
| 8 | 2.05 |

Hence,

$$V_T^{2} = 2\Psi_o \ln\left(T_{fa}\, B_{if}\right) = \frac{2(6.35 \times 10^{-3})(1.57 \times 10^{3})}{42.2} \ln 2.2 \times 10^{6}$$

$$(3.15 \times 10^{3})$$

or $V_t = 3.8$ volts; thus, for the prescribed overall gain, the detection threshold is equal to 3.8 volts. Since the upper threshold was set at 10 volts, the maximum allowable gain per stage is 10/3.8 = 2.6. It is seen by use of Table I-3 that there must be at least seven video amplifier stages: one stage with a voltage gain of 5.0 and six stages with a voltage gain of 2.61.

The output noise of the final video amplifier will be amplified, band-limited, and used to control the gain in the IF amplifier. The bandwidth of the noise automatic gain control is not critical. The two requirements are (1) it must not respond to the video pulse when a target reflection is received, and (2) the setting of the proper gain in the IF amplifier to hold the rms noise voltage constant relative to the detection threshold voltage must be accomplished in a few seconds. A 0.1-Hz noise bandwidth meets both these requirements.

Each video amplifier stage is followed by a threshold device (T), a sample and hold circuit (S&H), a two-level, level detector (LD), and an output switch (S). The aggregate of these for all the video amplifiers comprise the voting circuits. Its function is exactly as implied: to sample the output of each video amplifier and pass the one that meets all the prerequisite requirements to the analog-to-digital converter for quantization. The detail operation is as follows.

A video output that is greater than or equal to the detection threshold (3.8 volts) will cross the threshold. This will signal the sample and hold to store the peak value of that signal. The sample-and-hold is reset to zero on each transmit pulse ($T_o$). The two-level level detector for each video channel then samples the dc level stored in the sample-and-hold, and if it is between 3.8 and 10 volts, it signals the output switch to pass the level through the output switch. If it is less than 3.8 volts or greater than 10 volts, the level detector senses this and signals the output to remain closed and not to pass the dc level. Thus, the choice or vote is automatic. Also, due to gain drifts, there must be some spread in the upper threshold to assure detection. For this case, it would be possible for there to be two correct indications at the level detector. The circuitry is implemented such that the signal with the largest signal-to-noise ratio only will be passed for parameter quantization.

5. Synchronizer and Parameter Quantizer Description

The synchronizer and parameter quantizer contain the basic clock, registers, and logic to synchronize the system and to convert time, amplitude, and angles into digital words. Consider first the range counter illustrated in Figure I-17.

When the RF pulse is transmitted, the same pulse from the modulator is used to "set" the three flip-flops. This allows the clock to "toggle" the three N-stage counters. If a detection threshold is exceeded, the flip-flop corresponding to that set of channels is "reset," disconnecting the clock from the counter. The digital word now stored in the counter is proportional to the range to the detected particle. If large particles were detected at close range, there would be a range number stored in each of the N-stage counters. Thus, the question is why use three range counting registers?

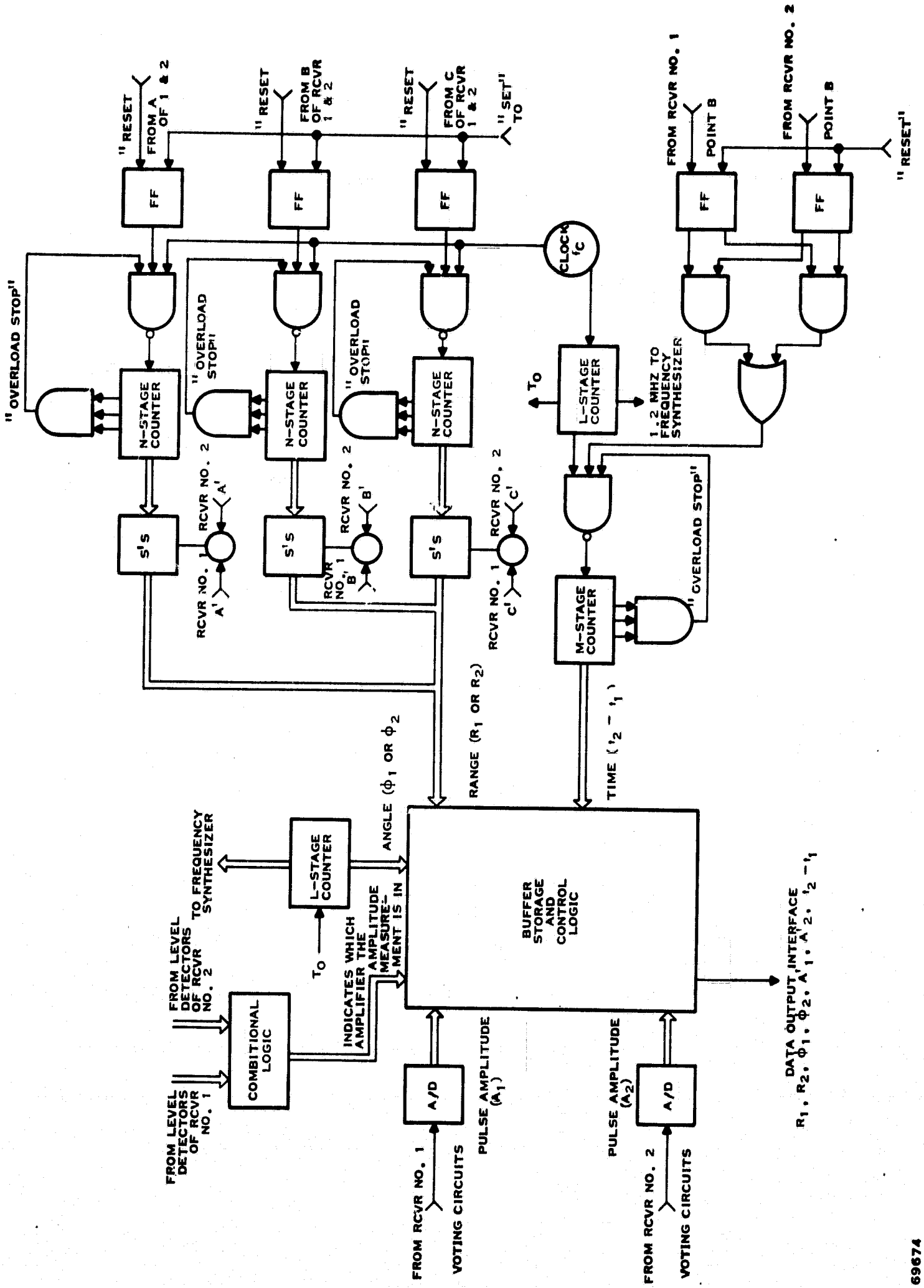


Figure I-17. Synchronizer and Parameter Quantizer

It was shown in the error analysis section that rms error of a fraction of a pulsewidth in range would cause large errors in the estimation of the particle cross section. If, as in the case above, the range is measured with respect to the threshold crossing of a saturated video amplifier, range errors in excess of the pulsewidth could occur. This would, in turn, cause excessive errors in the estimation of the particle cross section. By use of three range counters the measurement will always be accomplished by a nonsaturated video amplifier and the errors due to nonoptimum pulse amplitude threshold levels can be removed. The choice of which three estimated radar ranges to use is determined by the same method as the amplitude choice described in the previous section.

Consider now the measurement of the travel time of a particle from one beam to the other beam. This requires two separate receiver channels or some method to distinguish between returns from the separate beams. Within the parameter quantizer, the return from one beam is used to set a bistable multivibrator which allows the counter to "toggle" the M-stage counter. If more returns are received from this same beam, no change occurs. When a return is received from the other beam, a second bistable multivibrator is set disconnecting the clock from the M-stage counter. Thus, the word stored in the M-stage counter is proportional to the particle travel time between the two separate beams.

The final parameter to be quantized is the beam pointing direction. Since we are considering the case for two separated scanning beams, the beam separation angle (10 degrees) is a fixed quantity and the receiver need only measure the angle within the scan plane. This result is readily available since the quantizer will send a digital word to the frequency synthesizer to tell it to point to a particular direction. This same word may be used to transmit the pointing angle to buffer storage. Another possible method which will reduce the number of interconnecting wires would be to initialize the registers of both the quantizer and synthesizer to a particular angle and then step the beam contiguously by stepping the appropriate register. The registers would be reset when the total number of scan positions had been completed. Thus, the only interconnection wires needed would be "set," "reset" and "step."

Consider the number of stages required for each counter. Basically, we wish to quantize with as few a number of bits as possible while maintaining the measurement accuracy. Quantizating errors generally have a uniform probability distribution. The rms error for such a distribution is given by

$$\sigma_Q = \frac{b - a}{2\sqrt{3}}$$

where b is the maximum possible error and a is the minimum possible error; also, a and b have the same units as Q. Thus, given the frequency of the clock, the quantizing error for the range reading, assuming the average value [(b + a)/2] is zero, is given by

$$\sigma R_q = \frac{c}{2f_c\sqrt{3}} \text{ meters}$$

where c is the speed of light in meters per second and $f_c$ is the clock frequency in Hertz. It is also evident that the standard deviation in time is given by

$$\sigma T_q = \frac{c}{f_c\sqrt{3}} \text{ meters}$$

Thus, given the range of time error due to noise or whatever may cause them, the value of the above expression should be approximately ten times smaller.

The above technique will be used to determine the value, in time or equivalent range, of the least significant bit. The total number of bits in the counter can now be ascertained if the maximum range and maximum time that it is required to measure are known. Since the value of the least significant bit ($N_o$) and the maximum number of the counter must be able to measure and store ($N_m$), the number of bistables or bits (n) is given by

$$n = 3.33 \log (N_m/N_o)$$

where n must be rounded off to the next largest integer. It is also advisable to add one more bit to provide an overload stop. Then if the counter becomes completely loaded it will stop and not continue counting from the least significant bit.

Consider the determination of the amount of quantization required based upon the error analysis and the system optimization specification. In this determination, only maximum and minimum values need be used as they set the constraints upon the data quantization. For a beam separation of 10 degrees, these values are

Maximum detection range ($R_{max}$) = 7500 meters

Minimum detection range ($R_{min}$) = 200 meters

Maximum travel time ($t_{max}$) = $55 \times 10^{-3}$ seconds } between beams

Minimum travel time ($t_{min}$) = $2.5 \times 10^{-3}$ seconds } between beams

Number of scan position ($S_p$) = 50

Maximum amplitude ($A_{max}$) = 10 volts

Minimum amplitude ($A_{min}$) = 3.8 volts

Transmit pulsewidth ($\tau$) = $0.5 \times 10^{-6}$ seconds
= 75 meters (two way)

Pulse repetition frequency (prf) = 20 kHz.

In the error analysis, it was shown that for near ranges the range accuracy was set by the pulsewidth to detection range ratio ($\tau/R_o$). Hence, by setting the range quantizing error to be 0.1 of $R_o$, namely 7.5 meters, it will have only a small effect on the range accuracy. Therefore, one finds that

$$f_c = \frac{3 \times 10^8}{2(7.5)(1.732)} = 11.5 \times 10^6 \text{ Hz}$$

and that the least significant bit is equal to 13 meters in range and equal to $8.7 \times 10^{-8}$ seconds in time. From this one finds that the number of bits for each range register is

$$r = 3.33 \log \quad 7500/13 = 9.1 \leq 10 \text{ bits}$$

and using the same basic clock, the number of bits for the time counter is

$$t = 3.33 \log 55 \times 10^{-3}/8.7 = 10^{-8} = 19.3 \leq 20 \text{ bits}$$

This is an excessive number of bits for the accuracy of travel time measurement above. From the error analysis, the required clock frequency is found to be

$$\left[\sqrt{6}\,(0.01)(2.5 \times 10^{-3})\right]^{-1} = f_c = 16 \text{ kHz}$$

Thus, the system prf would be a sufficient clock rate for the particle travel time counter and the number of bits now required is

$$n_{tz} = 3.33 \log (55 \times 10^{-3})(20 \times 10^{-3}) = 10.1 \text{ bits} < 11 \text{ bits}$$

The synchronizer must supply a frequency of approximately 1.2 MHz to the frequency synthesizer. These can readily be obtained from a single system clock. Thus, the basic clock will be divided by 512 (nine bistables) to obtain the prf; this will also be the clock for the particle travel time between beams. The particle travel time counter will require 11 bits. At the appropriate points in the divide-by-512 counter, the 1.2-MHz wave will be picked off, buffered, and hard-wired to the synthesizer. This type of mechanization requires only one basic clock as opposed to three (prf, $f_c$, and 1.2 MHz) if divider chains are not used.

The number of bits required to specify the 50 scan positions is

$$n_s = 3.33 \log 50 = 5.65 = 6.0 \text{ bits}$$

The quantization volt ge for the pulse amplitude is not critical. It was shown in the error analysis that the largest error in measuring cross section was due to the lack of good angle prediction. It was also shown in the error analyses that when the particle is directly on boresight and the ratio of $\tau/T$ is small, the normalized error is 20 percent. Thus, the quantization error ($\sigma_{ag}$) will be set to be 5 percent of the amplitude and it is found that

$$\sigma_{ag} = \frac{a}{2\sqrt{3}}$$

where a is the quantized voltage segment. However, a is equal to $(A_{max} - A_{min})/$ where k is the number of voltage segments. Thus,

$$\sigma = \frac{A_{max} - A_{min}}{2k\sqrt{3}}$$

and letting $\sigma$ be $0.05\ A_{ave}$, one finds that

$$0.05\ A_{ave} = \frac{A_{ave}}{4k\sqrt{3}} = k = \frac{1}{0.05(4)\ (\sqrt{3})} = 2.886 \leq 3$$

and that the quantized interval is $\frac{A_{max} - A_{min}}{k} = a = \frac{16 - 3.8}{3} = 2.067$ volts. Therefore, the amplitude quantization will require only 2 bits, i.e., $2^2 = 4$, where only a number of 3 is required. Hence, with no increase in required power or electrical components, the actual quantizing level could be $\frac{10 - 3.8}{4} = 1.55$ volts. This will indicate the output level of the amplifier. There must also be an indication of which mplifier in the chain is providing the measurement. Since there are a total of seven separate amplifiers this would require three bits. This sums to a total of 5 bits for the amplitude digital word.

Summarizing the required digital word lengths, it was found that the range word is 10 bits per register, the time word requires 11 bits, the scan requirement implies a need for 6 bits, and the amplitude requires 5 bits. This sums to a total of 32 bits of information for each detection.

The final unit to be discussed in the parameter quantizer and synchronizer is the buffer storage. It is possible that the raw data could be used to compute the characterizing parameters, i.e., $\sigma$, V, $\alpha$, and $\beta$. This data then could be transmitted to earth. As a rule of thumb, if the transmitted data cannot be compressed by a factor of 10, it is best to send the raw data.

The raw data consists of the following parameters.

| | |
|---|---|
| $R_1$ (range to particle in beam 1) | 10 bits |
| $R_2$ (range to particle in beam 2) | 10 bits |
| $\phi_1$ (beam 1 pointing angle) | 6 bits |
| $\phi_2$ (beam 2 pointing angle) | 6 bits |
| $A_1$ (video pulse amplitude in beam 1) | 5 bits |
| $A_2$ (video pulse amplitude in beam 2) | 5 bits |
| $(t_2 - t_1)$ (particle travel time between beams) | 11 bits |
| Total | 53 bits per particle |

Since it would be virtually impossible to send all the characterization parameters with five bits, no computer will be used. Thus, the buffer storage will contain a 53-bit register and the necessary logic to shift the data in and out. Several such registers could be provided on the change that several detections may be made in close proximity.

6. Built-In Test Equipment And Calibration

Because of the long duration of the mission for this equipment, it is an advantage to include in the system a large number of test points, built-in test equipment, and calibration points. These points are invaluable for failure analysis, fault location, and determination of degradation of the system as a function of time. Since the particle detection rate is small in quantity, the data storage register will be empty most of the time. Thus, the basic test points could be sampled and quantized by the same equipment as the pulse amplitude and the same data storage could be utilized. The increase in system complexity would therefore include the addition of a switching commutator to connect the proper points to the analog-to-digital converter, a small amount of logic for identification, and to switch back to particle characterization if a detection occurs while in a testing mode and the addition of the test points.

The test points are an integral part of each functional block. Extreme care must be taken to assure that the test point does not affect the operation of the functional block and that the voltage or current reading at the test point is a true indication of the operational state of the functional block. A list of recommended test points and test functions include:

One for each of the low voltage and high voltage power supplies.

Crystal current (voltage) to check the local oscillator and mixer performance.

A small resistor and hold circuits in the TWT supply to check for tube transmission and the approximate output power.

The noise automatic gain control voltage to check the approximate sensitivity and variations thereof.

Prime power at the radar unit to check for excessive load current or lack of prime power.

An ac-to-dc frequency sensitive filter on the basic clock to check for proper operation and frequency.

Temperature sensors in selected portions of the radar.

The voltage applied to each subfrequency synthesizer VCO to check for proper operation.

Other test points could be added but the ones listed above should be considered the minimum for fault isolation failure analysis and calibration.

## D. RELIABILITY ANALYSIS

### 1. Introduction

This section presents the results of the reliability analysis. Indices used in measuring reliability are discussed and the mathematical bases for reliability calculations are presented in Appendix A.

The reliability prediction with associated conditions and assumptions is followed by a design evaluation from a reliability standpoint, and environmental factors affecting reliability are discussed. The constraints of the meteoroid radar mission indicate that mission reliability is the most meaningful index and it will be used herein.

### 2. Reliability Prediction

#### a. Conditions and Assumptions

It is assumed that the meteoroid radar heat transfer system will maintain the equipment operating environment at approximately 40°C ambient; use of heat pipe cooling techniques is assumed in controlling TWT heating. The device failure rates are determined based on a 40°C ambient temperature.

Historical failure data from a system which operated in a deep space environment for three years continuously at 40°C ambient is used where applicable.

State-of-the-art device failure rates experienced or compiled by Texas Instruments reflecting improvements expected by 1973 are used. Reasonable use of integrated circuits, including large and medium scale, is assumed.

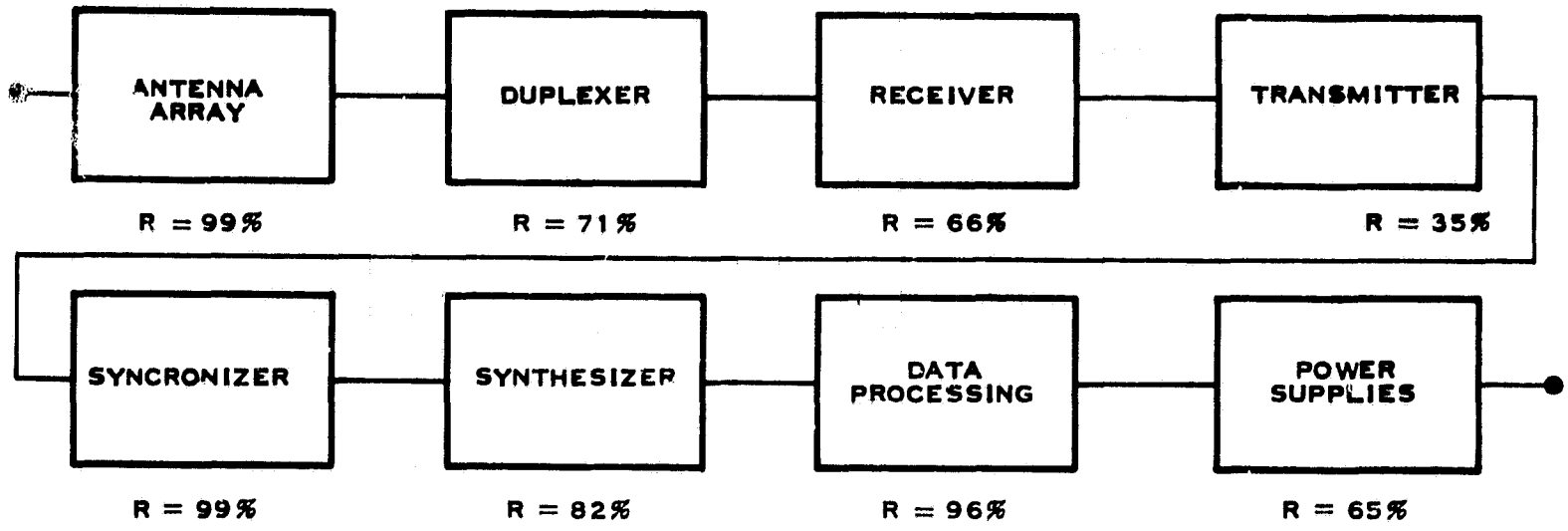


Figure I-18. Meteoroid Radar System Reliability Model

The use of high reliability devices is assumed based on the following procedures: (1) devices screened (i.e., burned-in), and (2) standard derating practices used.

Meteoroid and radiation damage are assumed to be insignificant and mechanical vibration is assumed to be moderate

Mission reliability is calculated for a one-year, 8760-hour, continuous operating time, and consideration is given to the effects of dormant periods and on-off cycling on system reliability. It is assumed that the radar payload achieves orbit and that no reliability degradation results from launch and orbit achievement.

b. Model/Discussion

Figure I-18 presents the system reliability model by functional blocks. The antenna array was assumed to have no time-dependent failure components, and therefore its reliability is a one-shot probability of successful deployment. Through analysis of typical explosive, spring-loaded deployment systems, the probability of successful deployment is estimated to be 0.99. The remainder of the functional blocks reflect devices with essentially constant failure rates as a function of time.

Figure I-19, solid line, shows the reliability-versus-time profile for the continuously operating system. The reliability degradation is exponential. Since this system probably will be dormant for a portion of the time, either before initial energizing or in on-off cycling, the effects of dormancy need to be considered. The predicted effects of dormancy and on-off cycling are covered in Subsection 4, Environmental Factors.

The use of redundancy would improve the system reliability figure significantly. The antenna structure, which would not benefit from redundancy, accounts for roughly 50 percent of the total radar system weight. Incorporating single-element redundancy where practical and feasible in the remainder of the system would only add about 35 percent more system weight but would provide a significant reliability increase. At the one-year point a reliability of 38 percent is predicted as opposed to 8 percent (Figures I-20 and I-19) for the nonredundant system. At the 4500-hour point, a 33 percent reliability improvement for the redundant system over that of the nonredundant system is predicted. The MTBF for the redundant system is predicted to be 9090 hours.

Figure I-20 is based upon using instantaneous equivalent failure rates evaluated at the one-year operating time for the redundant portions of the system. For this system the approximations yield the most accurate failure rates for the redundant portions and when these failure rates are added to those of the serial portion, system MTBF can be calculated through the reciprocal relationship. The resulting curve of reliability versus time is therefore exponential. A detailed look at the reliability improvement possible through redundancy for various functional blocks in the system is presented in the following section.

### 3. Design Evaluation

This section evaluates the preliminary design from a reliability standpoint, pinpointing design problem areas and citing ways to improve reliability.

#### a. Transmitter

As seen from Figure I-18, the transmitter function has a reliability of 35 percent at the end of 8760 operating hours. The biggest single factor in this low reliability is the TWT. It accounts for approximately 30 percent of the total system failure rate. Figure I-19 shows the reliability gained by adding one TWT to the system for redundancy. Added weight, cost, and volume are trade-off considerations with the added reliability. Reliability of vacuum tubes is generally inversely related to the required average power output and frequency.

A comparison of the reliability and life of the TWT with other vacuum tube sources, in light of the required system parameter ranges, indicates that the TWT will offer the greatest advantages.

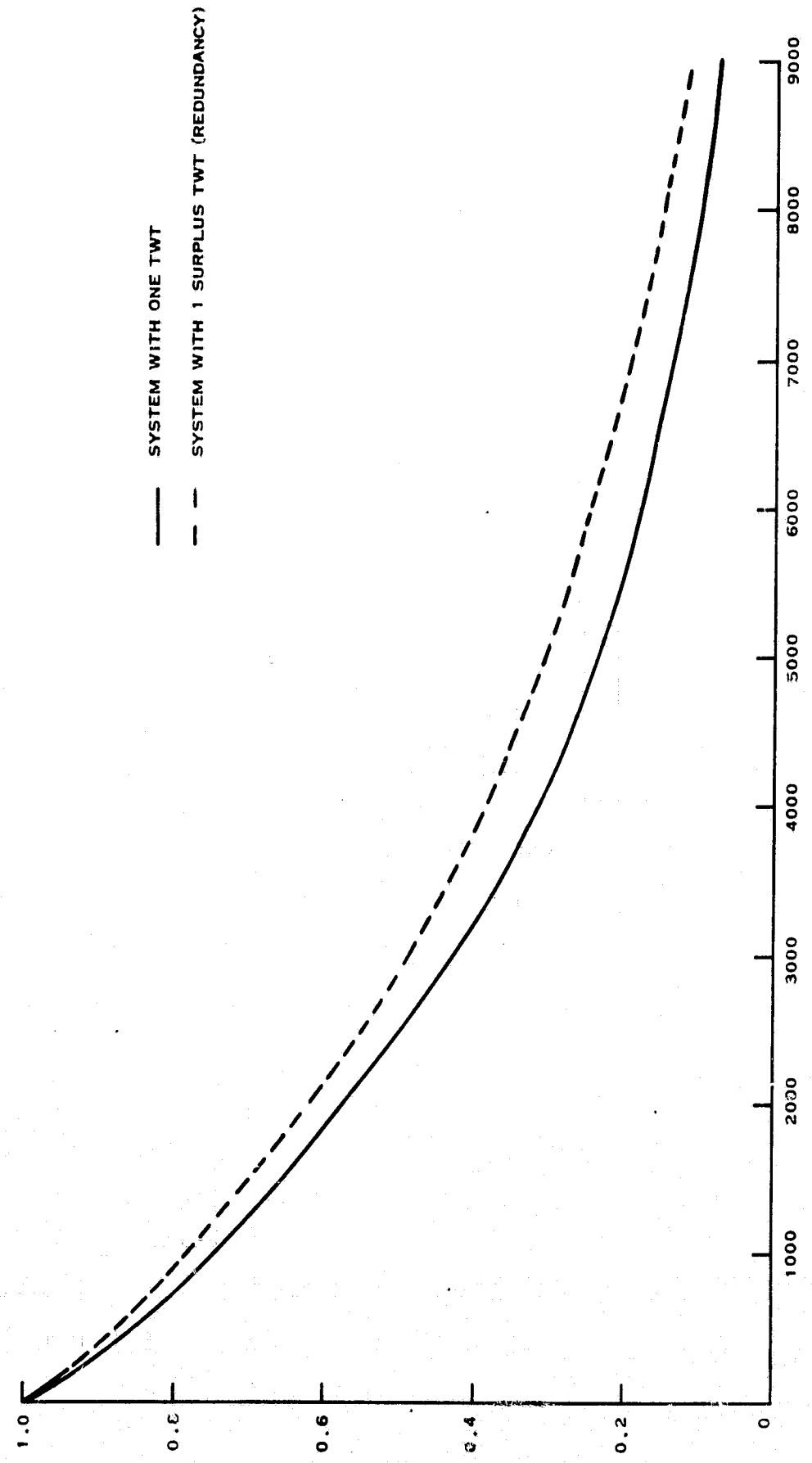


Figure I-19. System Reliability Versus Time

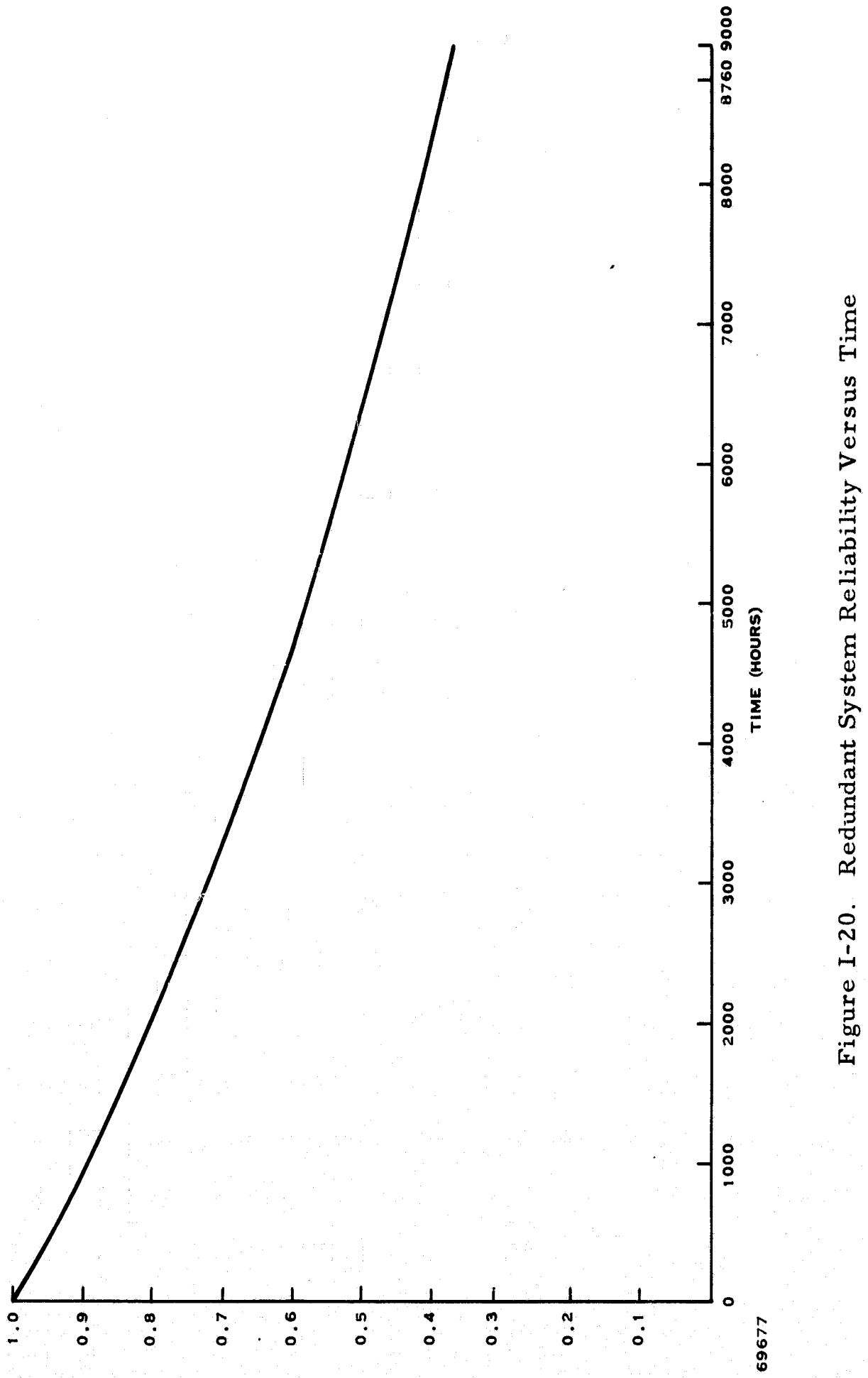


Figure I-20. Redundant System Reliability Versus Time

b. Power Conditioner

From Figure I-18 the power supply function reliability is 65 percent. Figure I-21 illustrates that a one-year reliability of nearly 100 percent can be obtained from an array of 12 power supplies of which three are surplus. This figure is based on a 1000-hour operating time and an individual module failure rate of 40 per $10^6$ hours. Figure I-21 is a computer-generated plot using Equation (5) for several different number of allowed failures, J.

c. Duplexer

The duplexer one-year reliability is 71 percent. This is primarily due to the failure rate contribution of the TR tubes, approximately 15 percent of the total system failure rate. Redundancy here, if feasible, would enhance reliability less than that of the TWT's.

4. Environmental Factors

a. Temperature

Since a 40° C ambient temperature and heat pipe cooling for the TWT are assumed based on historical date from a space environment, there do not appear to be any significant temperature effects on the reliability of internally housed components. Figure I-22 shows the effect of changes in ambient temperature on average component failure rate. Although the antenna array is mounted to the spacecraft body, since no electronic components are involved there should be no reliability degradation due to temperature.

b. Radiation

The threshold for radiation effects sufficient to degrade electronic and electromechanical parts is relatively high when compared to the radiation levels experienced in the normal space environment. For the orbits considered, no significant problems are expected. Table I-4 presents the types of degradation which could occur should radiation thresholds be exceeded as a result of overexposure to radiation.

Tests have shown that semiconductors are the most susceptible components to radiation degradation. Their radiation threshold is reached at approximately $10^2$ ergs/g. Other component radiation thresholds range from three to four magnitudes greater than the semiconductor.

As previously mentioned, equipment exposure is not anticipated for periods of time sufficient to exceed the minimum threshold.

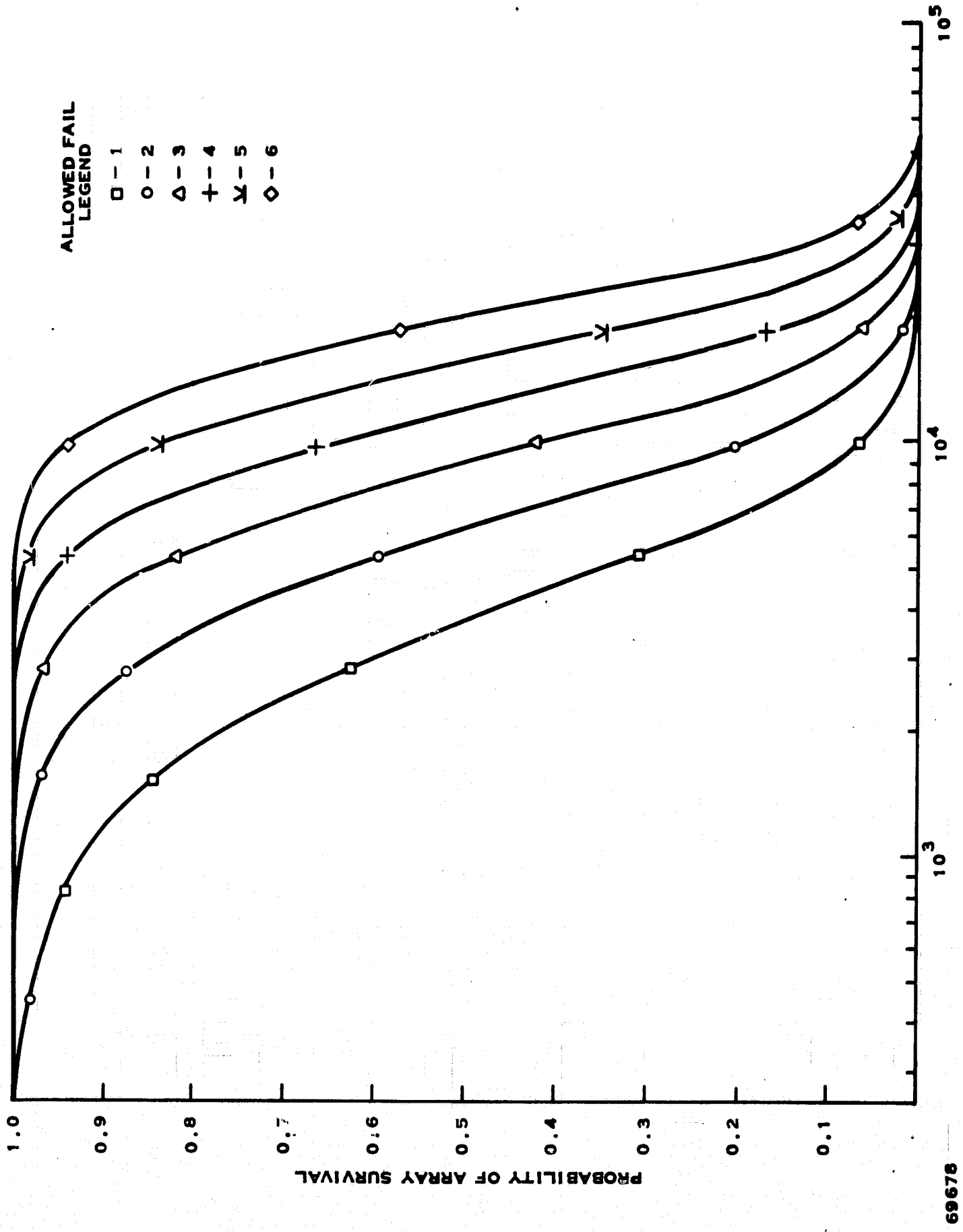


Figure I-21. Power Supply Array Survival Probability Versus Time for J-Allowed Failures

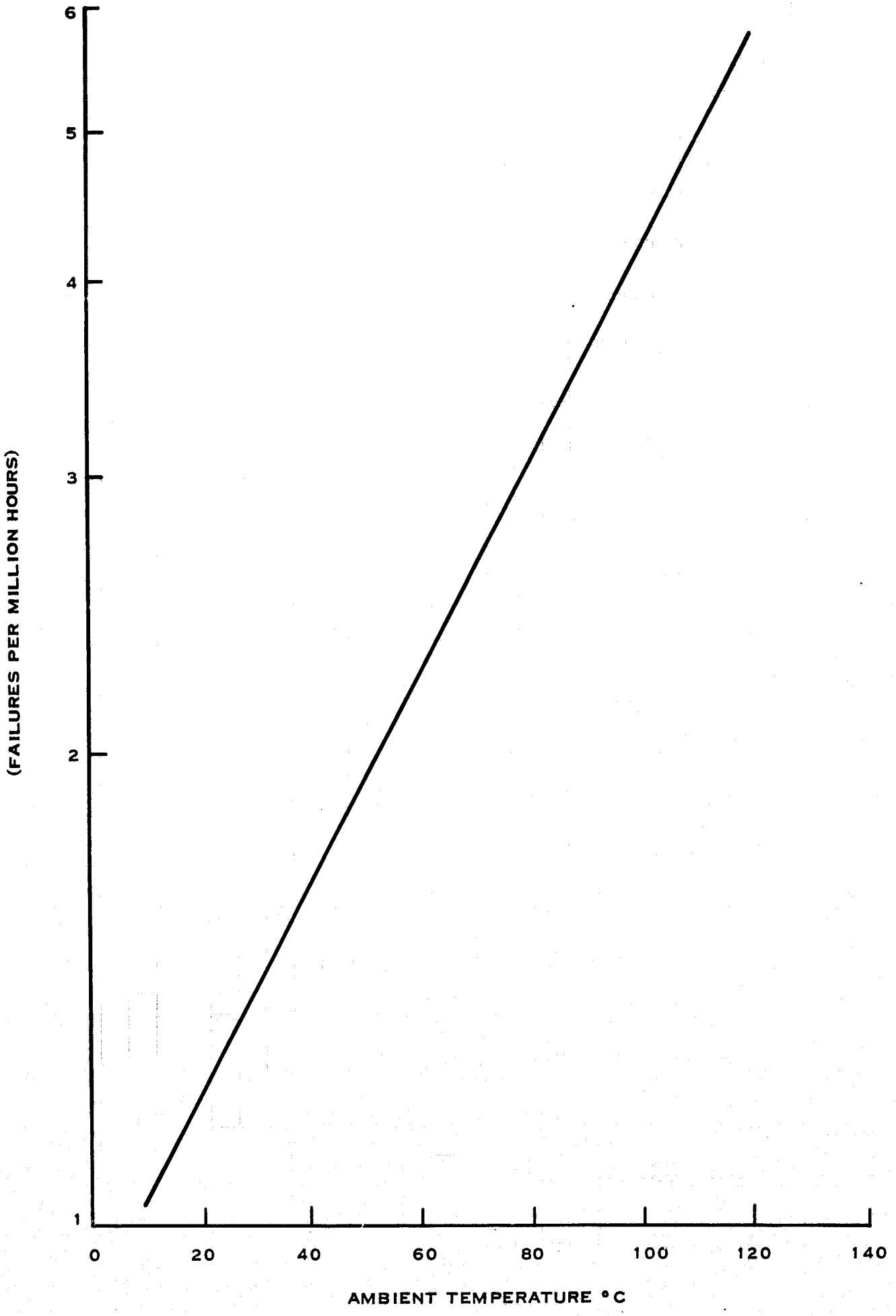


69679

Figure I-22. Average Component Failure Rate Versus Ambient Temperature*

For those periods in which it is exposed, the protection offered by the vehicle skin, structure, and system packaging normally will be sufficient to protect the equipment from radiation effects for a period of time far beyond the required equipment lifetime. In addition, the exposed antenna array is programmed to always face away from the sun, thus minimizing the effects of solar radiation. The effects of radiation on system component reliability in the deep space environment generally can be considered insignificant.

c. Shock and Vibration

Conditions associated with shock and vibration are not considered to be significant contributors to system unreliability for space equipments such as these conditions normally is encountered only during the launch phase. Good design practices developed as a result of extensive vibration testing have been proved adequate in controlling mechanical stressing during the launch phase.

Table I-4. Effects of Excessive Radiation

| Device Name | Effects |
|---|---|
| Antennas | Surfaces annealed, possible crystal growth, impurities migrated |
| Capacitors | Capacitance changed, dissipation factor and leakage increased |
| Coaxial connectors | Conductivity and leakage increased |
| Coaxial relays | Conductivity and leakage increased |
| Couplers, directional | VSWR and insertion loss changed |
| Diodes | |
| Switching | Highly susceptible to radiation, leakage current increased, minority carriers degraded |
| Varactor | Leakage current increased, minority carriers degraded |
| Zener | Leakage current increased, minority carriers degraded |
| Inductors | Possible insulation damaged, remanence and permeability reduced, coercive force increased |
| Junction boxes | Conductivity increased (ceramic insulator assumed) |

Table I-4. Effects of Excessive Radiation

| Device Name | Effects |
|---|---|
| Mixers | (Same effects as for semiconductors) |
| Resistors | |
| Composition | Possible resistivity changed, probably negative (resistance increased) |
| Film | Similar to aging, resistivity changed, probably positive (resistance reduced) |
| Wire-wound | Possible insulation damage |
| Solder joints | Possible whisker growth and crystalization |
| Transformers | Possible insulation damaged, remanence and permeability reduced, coercive force increased |
| Transistors | Leakage current induced, gain decreased |
| Traveling-wave tubes | Possible detuning and seal degradation |
| Solar cells | Transmissivity of cover glass changed, available power reduced, specular response changed, adhesive damaged |
| Mechanical components | Film layers including oxides removed, possible cold-welding if under pressure, some diffusion of metal to metal where intimate contact exists, surface annealed, possible crystal growth, some migration of impurities in parent metals, possible hydrogen embrittlement. * |

d. On-Off Cycling

The nature of the meteoroid radar system mission quite probably will imply that the radar set be turned off and on at various times during its lifetime. Therefore, it is important that the impact on system reliability resulting from on-off cycling of the equipment be evaluated.

Basically, two areas exist that should be considered in conjunction with on-off cycling; thermal cycling and circuit degradating resulting from transients and parametric drift during stabilization. Controls such as good design practices and extensive circuit testing have proved adequate to control the latter.

Improper application of thermal techniques may result in more serious problems in a space environment than would be encountered in a suborbital environment. Improper matching of electronic and electromechanical thermal coefficients, coupled with the continual thermal cycling experienced in the space environment, can result in continual internal and external stressing of components. Improper control of temperature excursions may result in the following effects: work hardening of material, sodium ion migration, chemical reaction due to impurities, and surface tracking. These effects of thermal cycling will, to a certain degree, be accelerated as a result of on-off cycling. Proper selection of materials and components, and good design and manufacturing practices, will maintain the reliability degradation rate to an insignificant level despite the mission time.

These conclusions are based on information contained in a report prepared for FARADA* pertaining to the subject of space vehicle equipment reliability. The report disclosed that a data encoder designed and built by Texas Instruments has operated in the space environment for approximately 27, 664 hours (three years) without failures or apparent degradation. Although this particular system has operated continuously, it is coupled with a transmitter which has been on-off cycled over the three-year period with no apparent reliability degradation.

e. Dormancy

Based on past analysis, on the average the ratio of operating to nonoperating failure rates is approximately 100 to 1. Assuming a duty factor greater than 10 percent, dormancy would not degrade system reliability any significant amount.

f. Meteoroids

As a result of probability calculations, it is not anticipated that contact will be made with any meteoroids large enough to cause system reliability degradation or put the system "off the air" instantaneously.

---

*FARADA—Failure Rate Data Handbook, published by the U. S. Naval Fleet Missile Systems Analysis and Evaluation Group.

### 5. Summary and Conclusions

The meteoroid radar set is generally a reliable system. Its system MTBF is quite respectable compared with other similar radar sets. The greatest single factor contributing to system unreliability is the 8760-hour operating time without maintenance. To achieve a reliability of 50 percent at the end of 8760 hours operation without maintenance, the total system failure rate would have to be $79 \times 10^{-6}$ failures per hour. This figure is extremely small for this type of system. Redundancy improves system reliability significantly (33 percent at 4500 hours of operation and 30 percent at 8760 hours) and yields a predicted MTBF of 9090 hours, or a little over one year.

Temperature, on-off cycling, vibration and shock, radiation, dormancy, and meteoroid environments were considered and within the stated assumptions none appeared to contribute significantly to system unreliability. Significant reliability improvement is achievable through use of large and medium scale, monolithic and hybrid integrated circuits in place of components; maximum use should be made of these IC devices.

Based on data from another deep space system, it is possible that the well designed, quality controlled meteoroid radar set will operate more reliably than the prediction indicates.

## E. SPACECRAFT INTERFACE REQUIREMENTS

### 1. Electrical Prime Power Interface

The electrical power interface and constraints are considered for both the Mariner '69 and the Voyager. Possible methods to increase the total prime power available are also considered based upon current work.

The Mariner '69 spacecraft is a Mars planetary orbiter in the weight range of 1000 pounds. It carries a relatively large number of planetary scan experiments including UV and IR scanners and two television cameras. Because of the high data rate capability of these instruments, the power system for Mariner '69 will be designed for the planetary orbit mode during which time the solar illumination is a minimum. A battery system will provide S/C power during the solar eclipse portion of the planetary orbit and the solar array must be sized to recharge the batteries during the illuminated portion of the orbit as well as providing S/C power. The solar array consists of four panels which are hinged to the spacecraft equipment ring. The Mariner '69 has approximately 83 square feet of solar panel with the limitation in size resulting from the volume restrictions of the Centaur/Surveyor nose fairing. If the solar panels are hinged at midchord as well as at the equipment ring, as has been suggested in alternate designs, the solar panel area may be increased to 127 square feet. Assuming a power conversion

efficiency of 10 percent and a cell packaging factor of 0.9, the maximum available power from the solar array is

$$P_{max} = \frac{0.14}{r^2} \text{ watts/cm}^2 \; (0.0)(0.9)(127 \text{ ft}^2)(6.45 \text{ cm}^2)(144 \text{ in}^2/\text{ft}^2)$$

$$= \frac{1488}{r^2} \text{ watts.}$$

Assume now that the identical spacecraft is intended for an asteroid belt mission having similar cruise mode power requirements. Thus, at r=2.9 AU. which is the sun-spacecraft distance corresponding to the peak data region for Mission 2,

$$P_{max} = 177 \text{ watts.}$$

During the interplanetary cruise portion of the mission, the S/C power requirement is as follows:

| | |
|---|---|
| Science | 27.6 |
| Data Encoder | 14 |
| Command Decoder | 8 |
| Central Computer and Sequencer | 16 |
| Control System Electronics | 39 |
| Pyro Control | 2 |
| Receiver TR | 17 |
| Central Unit | 2.1 |
| Exciter TR | 11 |
| Power Distribution Loss | 2 |
| Control Gyro and Electronics | 10 |
| Inverter Output = | 148.7 watts |

Assuming 85.7-percent efficiency, the required inverter input is 174 watts. Adding 5 watts for a power synchronizer gives 179 watts as the output from the main booster regulator. Assuming an 82.7-percent efficiency for the regulator gives 216 watts as regulator input. For a 20-watt transmitter radiated power, the RF power amplifier will use 85 watts. Allowing for 19 watts loss in the solar cell circuitry, the total power requirement is 320 watts. Thus, during the cruise mode of operation at 2.9 AU, there is a

need for 320 watts, not counting the radar need, but only 177 watts available. It is apparent that the current design cannot be easily converted to another mission even without the addition of the meteoroid radar system. Significant redesign would be necessary for Mission 2, the asteroid belt fly-through. Even Mission 1, the Mars fly-by, provides only 307 prime power watts at aphelion (2.2 AU).

If the current solar panel design consisting of a corrugated metallic substrate reinforced by spanwise beams is retained, little possibility exists for increasing the solar panel area. If the envelope of the shroud is increased by increasing the length of the cylindrical section of the nose fairing, the potential exists to increase the suggested two hinged panel areas to perhaps 150 square feet, but beyond this a new solar panel structural and deployment design will be necessary. Such an extension is not enough to add the radar to either mission.

The Voyager spacecraft is a planetary orbiter and an atmospheric entry capsule. The entry capsule weighs approximately 3000 pounds, the bus weighs approximately 2500 pounds, and the midcourse orbit adjust and retropulsion subsystems weigh about 12,000 pounds, giving a total S/C weight of about 17,500 pounds. The solar array is supported by annular disk structure supported by the S/C bus main equipment support ring. The structure is nondeployable and in the launch configuration extends to the Saturn shroud envelope. The solar panel area is 226 square feet with an active solar cell area of approximately 181.2 square feet. At 2.9 AU the maximum power available with the same assumptions as for the Mariner '69 array is 201 watts. During the cruise phase of the mission, the power requirement of the S/C is approximately 583 watts. The power capability of the Voyager can be easily increased three-fold by utilizing a deployable solar array structure without greatly changing the current S/C design. The radar would require 350 watts. Therefore, the solar cell must supply a total of 933 watts if a simple add-on is assumed.

The current demonstrated power-weight ratio of the solar cell array used on a Mariner S/C is approximately 10 watts per pound of solar array structure at earth distance. The corresponding weight-area ratio is 1 pound per square foot of solar array. Since the solar intensity varies as the inverse square of the sun spacecraft distance, at 2.9 AU the power-weight ratio is reduced by a factor of 8.4 to approximately 1.19 watts per pound. An array with a 1-kW output at 2.9 AU using proven array concepts would weight approximately 840 pounds and have an area of 840 square feet. These figures do not consider the UV degradation of the solar cells and the fact that a new solar panel structural design will be necessary to maintain the 1-pound per square foot figure while increasing panel area by an order of magnitude over present Mariner vehicles.

Studies currently are in progress to develop large area arrays with power-weight ratios of 20 watts per pound at 1 AU with the possibility of reaching 33 watts per pound for array total power of 50 kW at 1 AU. Encouragement for these designs has come from the need of a power source for a solar-electric spacecraft for missions with high energy requirements. Two design concepts with demonstration models presently under construction or planned for the near future appear definitely capable of achieving the 20-watt per pound figure. One of these consists of panels with a beryllium framework, either a truss or rigid frame, supporting a membrane consisting of crossed fiberglass tape which serves as a support for the solar cells. The panels must be folded in the launch configuration and deployed after insertion into orbit. One possible design employs a cable tie-down during launch and a cable deployment scheme for four main panels with an electric motor supplying the necessary energy. Subpanels are then deployed from the main panels by spring-damper devices. Another array concept utilizing lightweight hinged panels stows the panels in a tied down accordian configuration. Deployment is accomplished by cutting the tie-down cable with a pyrotechnic device which releases torsional spring-dampers at the hinge lines of the panels. The second array structural concept under study consists of a flexible solar cell support which may be rolled up on a drum. The structural support in the deployed position is supplied by a slit tube or a hat-shaped station section which is stored in an elastically strained flat configuration when rolled up but assumes a stiffened unstrained shape upon unrolling. At 2.9 AU the power-weight ratios of the 1 AU, 20- and 33-watt per pound arrays are 2.5 and 3.9 watts per pound, respectively, leading to array weights for a 1-kW solar array of 420 and 255 pounds, respectively. Note that the weight figures shown here do not include power conditioning equipment or secondary batteries. This would add perhaps 300 pounds to the power system for a 1000-watt solar array capacity.

In summary, the existing Mariner '69 or Voyager spacecraft designs cannot easily be modified to provide the prime power required by the suggested radar design for a deep space mission. The existing Mariner '69 design cannot even provide sufficient power for present power sinks for orbit locations slightly greater than those designed for. No easy modification should thus be expected for the significant prime power required by the modest radar set considered in this volume.

Spacecraft envisioned for the near future should easily be capable of providing the required prime power, provided the meteoroid radar system is considered a primary experiment package. For this reason a design providing modest detection capabilities and power requirements was selected for consideration. An add-on package having a prime power requirement consistent with that available from contemporary spacecraft on near earth missions would detect very little data according to the results of Volume I.

2. Data Relay Requirements

It was shown in Section C. 5 that to completely characterize the detected particle s parameters would require 53 bits per particle per detection. This information was obtained by considering the allowable quantization error and dynamic range of each parameter. If seven bits are added for identification of the separate parameters, a total of 60 bits per particle per detection is obtained.

The system analysis has indicated that there will be between 30 to 100 particle detections per year for a reasonable system power dissipation, i.e., approximately 320 watts. Thus, there would be only 6000 bits per year of the basic particle characterization data for spacecraft-to-earth transmission.

Consideration of the housekeeping functions of calibration, fault isolation, and failure analysis would add possibly another 6000 bits per year, since each test function need only be sampled every few days when all is going well. Therefore, this data will require no especial handling technique. It should be a relatively simple procedure to interlace 12, 000 bits of information per year with the data of the higher bit rate experiments.

## F. SYSTEM VOLUME, WEIGHT, AND POWER

Now the required system power, packaged weight, and volume will be approximated. The largest user of power is the transmitter tube and its associated circuitry. The Hughes 820H TWT was chosen as the primary power amplifier. It will be operated in the depressed collector mode to obtain a 20-percent dc-to-RF efficiency. The breakdown for the separate primary function of the transmitter-exciter, RF receiver, and the IF receiver is given in Table I-5. The size does not include any increase in packaged volume to account for any particular form factor, but the power dissipation does include the power supply efficiency and the power stated is the primary power requirement.

Table I-5. RF and IF Functional Requirements

| | Power Supplies | TWT and Exciter | Modulator | Mixer, TR and Isolators | IF Receivers | Total |
|---|---|---|---|---|---|---|
| Size ($in^3$) | 350 | 230 | 100 | 52 | 50 | 782 |
| Weight (pounds) | 18 | 23 | 5 | 6 | 3 | 55 |
| Power Dissipation (watts) | 22 | 200 | 10 | -- | 2 | 284* |

*Includes 50 watts radiated into space.

The remainder of the radar subsystem will be built with digital and linear integrated circuits and a small number of discrete components. The basic unit for the video amplifiers, comparators, sample and holds, and filter function will be a linear operational amplifier with a gain bandwidth of 40 MHz. These are readily available and require approximately 200 mW per amplifier. The switches, denoted S, would employ FET's because of the need for a high "off" impedance. These are also readily available and require 10 mW per switch.

The digital bistables and gates must have switching speeds of approximately 50 nsec. This is available for any of the standard logic: $T^2L$, ECL, or DTL. However, to reduce the packaged volume, MSI or LSI (medium scale integration or large scale integration) will be used and this is available only in $EC^2$ or $T^2L$. The $T^2L$ requires lower power per gate. Thus, the basic digital unit will be a $T^2L$ gate with a switching speed of 8 to 12 nano seconds per gate and a power requirement of 10 watts per gate. The characteristics of the remaining electronic subsystems are given in Table I-6. The distribution of components is given in the reliability section.

Table I-6. Electronic Subsystem Requirements

| | Video Receivers Unit | Parameter Quantizer and Synchronizer | Buffer Storage Unit | Frequency Synthesizer Unit | Total |
|---|---|---|---|---|---|
| Size ($in^3$) | 100 | 50 | 25 | 175 | 250 |
| Weight (pounds) | 3 | 1.5 | 0.5 | 2 | 7 |
| Power (watts) | 14.4 | 4.2 | 3.7 | 4.1 | 26.4 |

In Subsection C.1, the antenna was found to be 8 feet × 6 feet × 0.25 (average) foot or a total displaced volume of 12 cubic feet. The density of the epoxyglass honeycomb is 2.2 pounds per cubic foot; thus, it weighs 26 pounds. There will be an additional weight of 25 pounds for the metallized facing and adhesive, and 20 pounds for the deploying mechanism and hardware. Thus, the total weight is 71 pounds and an unfolded volume of 12 cubic feet.

A low power supply efficiency of 70 percent and a low power supply volume of 220 cubic inches are assumed. The total launch volume and weight and the cruise mode power are given in Table I-6; a form factor of 1.4 was used for the electronics packaging.

Table I-7. System Requirements

| | Electronics | Antenna |
|---|---|---|
| Volume ($ft^3$) | 1.0 | 81 |
| Weight (pounds) | 64 | 71 |
| Power (watts) | 320 | -- |

The folded volume of the antenna is a 6-foot diameter by 3-foot disk or 81 cubic feet (Table I-7).

# APPENDIX A

# MATHEMATICAL BASIS FOR RELIABILITY ANALYSIS

## I. RELIABILITY INDICES

The three most commonly used reliability indices are failure rate, mean-time-between-failure (MTBF), and probability of mission success (reliability or mission reliability). In many applications one index can be obtained from the other by a simple algebraic manipulation. In the meteoroid radar it is assumed that all functional blocks to which failure rates can be associated have constant failure rates; therefore, the simple relationships among MTBF, failure rate, and reliability hold. The basic relationships, valid for all cases, are given in Equations (A-1) and (A-2).

$$\text{MTBF} = \int_{t=0}^{\infty} R(t)\, dt \qquad \text{(A-1)}$$

$$\text{Failure Rate, } \lambda(t) = \frac{1}{R(t)} \frac{dR(t)}{dt} \qquad \text{(A-2)}$$

where R(t) is probability of equipment survival as a function of equipment operating time.

MTBF is single valued, while $\lambda$ and R are functions of time. Therefore, the MTBF of a system is significant only when either failure rate $\lambda$ is constant or when the equipment is to be used for operational periods of one or more multiples of MTBF (thus implying maintenance). When a large number of the equipments are being used for an operational time period less than an MTBF, the logistics of replacement or repair are of prime concern and failure rate as a function of time is the most significant reliability index.

When an important mission or task is to be performed by an equipment or system, the most significant reliability index is probability of mission success or reliability.

The constraints of the meteoroid radar mission indicate that mission reliability is the most meaningful index, while MTBF can also be used. Mathematical bases of reliability for the constant failure rate case and for the case of partial redundancy used for reliability enhancement are presented in the following section.

## II. MATHEMATICAL BASES

### A. Constant Failure Rate

If failure rate $\lambda$ [(t) is constant (i.e., failure of any part of the system causes radar failure)], reliability is given by Equation (A-3).

$$R(t) = e^{-\lambda t} \tag{A-3}$$

From Equation (A-3) it can be seen that increasing t decreases reliability exponentially. The assumption of constant failure rate is valid for most parts and circuits.

### B. Partial Redundancy

If J elements of an array of N elements may fail without causing array failure, then array reliability is given by Equation (A-4).

$$R_a(t) = \sum_{i=0}^{J} \binom{N}{i} R_e^{(N-i)} (1 - R_e)^i \tag{A-4}$$

where $R_e(t)$ is the reliability of a single array element. Usually element failure rate is constant and $R_e(t)$ is given by Equation (A-3). Equation (A-4) can then be written as

$$R_a(t) = \sum_{i=0}^{J} \binom{N}{i} e^{-(N-i)\lambda_e t)^i} (1 - e^{-\lambda_e t})^i \tag{A-5}$$

For relatively simple functional blocks the above equation is sufficient, but if larger arrays are involved, unwieldy calculations arise even for a computer. To alleviate this problem, use is made of statistical techniques leading up to utilization of the standard normal table for obtaining probability of success.

### C. System Reliability

Overall system reliability is given by Equation (A-6).

$$R_s(t) = \prod_{i=1}^{n} R_i(t) \tag{A-6}$$

where the $R_i(t)$ is given by either equation (A-3) or Equation (A-5) depending on whether or not redundancy is utilized.